Methods xxx (2015) xxx–xxx

Contents lists available at ScienceDirect

Methods

journal homepage: www.elsevier.com/locate/ymeth

Design and construction of conformational biosensors to monitor ion channel activation: A prototype FlAsH/BRET-approach to Kir3 channels

Derek N. Robertson [a,1], Rory Sleno [b,1], Karim Nagi [a,d], Darlaine Pétrin [b], Terence E. Hébert [b], Graciela Pineyro [a,c,d,e,*]

[a] CHU Ste-Justine Centre de Recherche, Montreal, Quebec, Canada
[b] Department of Pharmacology and Therapeutics, McGill University, Montreal, Quebec, Canada
[c] Department of Psychiatry, Université de Montréal, Montreal, Quebec, Canada
[d] Department of Pharmacology, Université de Montréal, Montreal, Quebec, Canada
[e] Department of Neuroscience, Université de Montréal, Montreal, Quebec, Canada

ARTICLE INFO

Article history:
Received 25 May 2015
Received in revised form 15 July 2015
Accepted 20 July 2015
Available online xxxx

Keywords:
BRET
Kir3 channels
Biosensor
High throughput screening
Fluxor®
Nano-Luc (NLuc®)

ABSTRACT

Ion channels play a vital role in numerous physiological functions and drugs that target them are actively pursued for development of novel therapeutic agents. Here we report a means for monitoring in real time the conformational changes undergone by channel proteins upon exposure to pharmacological stimuli. The approach relies on tracking structural rearrangements by monitoring changes in bioluminescence energy transfer (BRET). To provide proof of principle we have worked with Kir3 neuronal channels producing 10 different constructs which were combined into 17 donor–acceptor BRET pairs. Among these combinations, pairs bearing the donor Nano-Luc (NLuc) at the C-terminal end of Kir3.2 subunits and the FlAsH acceptor at the N-terminal end (NT) or the interfacial helix (N70) of Kir3.1 subunits were identified as potential tools. These pairs displayed significant changes in energy transfer upon activation with direct channel ligands or via stimulation of G protein-coupled receptors. Conformational changes associated with channel activation followed similar kinetics as channel currents. Dose response curves generated by different agonists in FlAsH–BRET assays displayed similar rank order of potency as those obtained with conventional BRET readouts of G protein activation and ion flux assays. Conformational biosensors as the ones reported herein should prove a valuable complement to other methodologies currently used in channel drug discovery.

1. Introduction

Ion channels comprise 1.5% of the human genome and are involved in numerous physiological functions including nerve and muscle excitability, hormone secretion, bone remodeling, immune response and cell proliferation [1]. Because of their implication in such variety of functions, drugs that modulate channel activity can be used for treating a wide range of pathological conditions spanning all major therapeutic areas. It is not surprising then, that multiple approaches have been developed to monitor how channel activity may be modified by potentially therapeutic agents.

Among available techniques, electrophysiological assays have remained the gold standard for directly assessing drug effects on channel proteins and, at present, patch clamp is the only means for characterizing these effects in real-time. Although, the number of drugs that can be assessed with this physiologically relevant readout has constantly improved [2], it is also undeniable that cell-based assays allow to handle significantly larger volumes of compounds and are more suited for initial steps of screening campaigns. The most frequently used cell-based assays rely on measurements of ion flux or on the use of voltage-dependent dyes, which constitute indirect readouts far removed from the channel protein [3]. As a consequence, the number of false positives and negatives they yield remains high, reducing the efficiency of cell-based screening methods. Here we developed and validated a methodology for monitoring conformational dynamics of channel

Abbreviations: BRET, Bioluminescence Resonance Energy Transfer; FlAsH-EDT$_2$, fluorescein arsenical hairpin binder-ethanedithiol; TC, tetracysteine; Kir3/GIRK, G protein-gated inwardly rectifying potassium channels; RLuc, *Renilla* luciferase; NLuc, Nano-luciferase; δOR, δ-opioid receptor; CTD, C-terminal domain; NTD, N-terminal domain; TMD, trans-membrane domain.

* Corresponding author at: 3175 Côte Ste-Catherine, Montreal, Quebec H3T 1C5, Canada.
E-mail address: graciela.pineyro.filpo@umontreal.ca (G. Pineyro).

[1] Contributed equally to this publication.

http://dx.doi.org/10.1016/j.ymeth.2015.07.011
1046-2023/

gating in real time. To capture these conformational changes we have built biosensors that monitor structural rearrangements which take place within or among channel subunits via changes in bioluminescence energy transfer (BRET). This is a cell-based protein imaging technique that not only senses subtle conformational changes but provides the basis for eventual use of this type of biosensors in a high-throughput assay format.

To provide proof of principle that conformational dynamics constitutes a viable readout for identification of channel modulators we have worked with inwardly rectifying K^+ channels that are modulated by G proteins (GIRK or Kir3) [4]. Donors *Renilla*-Luciferase (RLuc) or Nano-Luciferase® (NLuc) were engineered into the C-terminus of Kir3.1 or Kir3.2 subunits, and the TC-domain (CCPGCC) that binds the FlAsH acceptor was introduced at selected positions in the same or different subunits as the donor, so as to respectively yield intra- or intermolecular biosensors. Engineered constructs were validated in terms of membrane expression and ability to conduct current. Once fully validated, donor–acceptor pairs were used for characterization of their BRET responses. BRET changes associated with channel activation followed similar kinetics as the currents generated by activators, and pharmacological responses of biosensor pairs were in agreement with known pharmacology of tested ligands.

Cell-based, conformational BRET biosensors should prove complementary to techniques currently use for monitoring channel function and offer new possibilities for identifying and/or developing channel modulators.

2. Materials and methods

All chemicals were purchased from Sigma, unless otherwise mentioned. Antibodies were mouse Anti-Flag M1 (F3040), Anti-Kir3.1 (Alomone Labs, APC-005), Anti-Kir3.2 (Alomone Labs, APC-006) and rabbit Anti-Flag (F7425). Secondary antibodies were Anti-mouse IgG Alexa 488 (Invitrogen, A21202), Anti-mouse IgG Alexa 594 (Invitrogen, A11005), Anti-rabbit IgG Alexa 488 (Invitrogen, A11034), and Anti-rabbit IgG Alexa 594 Invitrogen, A21207). Mouse δOR with a Flag tag at the N-terminal (m-Flag-δOR) was a kind gift from Dr. Mark Von-Zastrow [5]. The TC-RLuc construct and human Kir3.2-RLuc were as previously described [6].

2.1. Drugs

AR-M 1000390 (AR-M 390) (R&D Systems), Deltorphin B (AnaSpec), Met-Enkephalin (AnaSpec), SNC-80 (Tocris), [D-Pen^2, D-Pen^5]Enkephalin (DPDPE) (Tocris), ML-297 (Cayman Chemical Company).

2.2. Construct design and construction

2.2.1. Constructs containing the TC-domain allowing for FlAsH-EDT$_2$ binding

TC-domain containing constructs were made for the human Kir3.1 subunit also containing the BRET donor RLuc [7]. The 5 constructs made in this fashion were NT-TC-Kir3.1-RLuc (NT); N20-TC-Kir3.1-RLuc (N20); N70-TC-Kir3.1-RLuc (N70); Kir3.1-TC-βBβC-RLuc (βBβC) and Kir3.1-TC-βGβH-RLuc (βGβH) (Section 2.2.1.1).

A second round of cloning allowed for the construction of TC-domain containing Kir3.1 subunits without the RLuc internally, but when paired with the Kir3.2-Luc, permitted the monitoring of BRET between channel subunits. Five constructs were made in this fashion: NT-TC-Kir3.1 (NT); N20-TC-Kir3.1 (N20); N70-TC-Kir3.1 (N70); Kir3.1-TC-βBβC (βBβC) and Kir3.1-TC-βGβH (βGβH) (Section 2.2.1.2). Constructs generated in this study are summarized in Table 1.

2.2.1.1. Constructs containing RLuc and TC-domain tags for performing intra-molecular BRET. The NT constructs were built using a standard single PCR technique, with the forward primer to insert the FlAsH tag upstream of the channel subunit sequence. For constructs with the FlAsH tag inserted within the channel subunit sequence, an overlapping PCR technique was used. Briefly, Kir3.1 was amplified by PCR using a Kir3.1-GFP10 plasmid available in our laboratory (Kir3.1 from the Kir3.1-RLuc plasmid was subcloned into a pGFP10 vector). While the 3′ ends of the primers used for first round reactions are complementary to the template DNA, the sequence tgctgccccggctgctgc (human preferred codons for CCPGCC) was added at their 5′ ends. This produced two fragments consisting of the 5′ end of Kir3.1 with the TC tag at the 3′ end or the TC tag at the 5′ end and the remaining Kir3.1 sequence at the 3′ end. The fragments were then mixed and allowed to anneal, and served in a second round PCR to generate a full receptor coding sequence with the TC tag inserted within the sequence of Kir3.1. The PCR product from the second round was then ligated into an accepting vector (pRLucN2) containing RLuc at the 3′ end of the insertion. Constructs were bidirectionally sequenced using CMV forward and RLuc reverse primers (detailed in Appendix 1).

2.2.1.2. Acceptor constructs for inter-molecular BRET. Kir3.1 constructs containing exclusively the TC-domain at various positions were produced following a similar strategy as the intra-molecular constructs above except a stop codon was introduced at the 3′ end of the Kir3.1 sequence. The second round PCR products were ligated into the pcDNA3.1+ vector. Constructs were bidirectionally sequenced using a T7 forward and BGH reverse primer (detailed in Appendix 2).

2.2.2. Kir3.2NLuc

This donor construct for inter-molecular BRET was prepared as follows. NLuc was amplified from pNL2.1 (Promega) using primers NotI NLuc FWD and NLuc ApaI RVS. The PCR product and the plasmid for human Kir3.2 in pcDNA3.1+ (a generous gift from Dr. Hubert Van Tol, University of Toronto [7]) were digested with NotI and ApaI. The digested PCR product and plasmid were ligated inserting the NLuc 3′ of the Kir3.2. The Kir3.2-Nluc construct was sequence bidirectionally using a T7 forward and BGH reverse primer. NotI NLuc FWD: 5′-aaaagcggccgccacaatggtcttcacactcgaa-3′; NLuc ApaI RVS: 5′-ttttgggcccttacgccagaatgcgttc-3′.

2.2.3. Kir3.2ΔNLuc

This truncated version of the Kir3.2-NLuc donor construct was produced in the following way. Kir3.2 was truncated at amino acid 380 using primers BamHI Kozak Kir3.2 FWD and Kir3.2trunc380 NotI RVS to amplify from the Kir3.2 in pcDNA3.1+ plasmid. The PCR product and Kir3.2NLuc were digested with BamHI and NotI. The digested PCR product and plasmid were then ligated, inserting the sequence coding for the truncated Kir3.2 5′ of the NLuc. The Kir3.2ΔNLuc construct was bidirectionally sequenced using a T7 forward and BGH reverse primer. BamHI Kozak Kir3.2 FWD 5′-aaaaaggatccgccaccatggccaagctgac-3′; Kir3.2trunc380 NotI RVS 5′-ttttttttgcggcggcgggcagctctgccctgctggctaact-3′.

2.2.4. TC-RLuc

This construct is a chimeric protein that codes solely for *Renilla* luciferase, with the TC-domain inserted at the C-terminal of the protein. This chimeric tool was useful for optimizing labeling conditions for the FlAsH-EDT$_2$, and BRET with the FlAsH-EDT$_2$-TC bound version of the luciferase, without need to worry about

Table 1
All Luc/TC Biosensor pairings tested.

Intramolecular	Intermolecular		
Kir3.1RLuc	Kir3.2RLuc	Kir3.2NLuc	Kir3.2ΔNLuc
NT	NT	NT	NT
N20	N20	N20	N20
βBβC	βBβC	βBβC	
βGβH	βGβH	βGβH	
N70 untested		N70	
		N70-RLuc	N70-RLuc

altered stoichiometry of transfecting all the various components of the biosensors we wished finally to construct [6].

2.3. Cell culture

Human Embryonic Kidney-293 (HEK 293) cells were cultured in Dulbecco's Modified Eagle Medium (Wisent) (10% Fetal Bovine Serum (FBS) (Wisent), 2 mM L-Glutamine 100 unit/ml Pen/Strep (Wisent)) at 37 °C in humidified atmosphere at 95% air and 5% CO_2. HEK293T cells were used specifically in electrophysiological assays for which they are the gold standard. BRET assays were carried out in HEK293SL cells since they detach less easily and were more adequate to wash away excess FlAsH after labeling.

2.4. Transfection with PEI

For transfection, HEK 293 cells were plated at 3.5×10^6 cells in 100 mm Petri dishes (Sarstedt), cultured for 24 h, then transfected as previously been described [8]. Briefly, cells were placed in serum-free DMEM, and plasmid DNA was mixed with NaCl (5 M, 15 μl/100 mm plate) and PBS. Polyethylenimine (PEI) (Polysciences Inc) of the calculated volume was added to a separate tube of phosphate-buffered saline (PBS), and the contents of the two tubes mixed. The optimal total plasmid DNA to PEI ratio was established by testing the following combinations: 1:2; 1:3; 1:4. The optimal ratio, where we measured the highest luminescence due to transfected RLuc, was found to be 1:4. After 20 min, the final DNA/PEI solution was added to the cells. Fours after transfection, the DMEM + 10% FBS was added to the cells, and the cells left for 48 h before experiments were carried out. Cells were transfected with m-Flag-δOR, $G\alpha_o$, $G\beta_1$, $G\gamma_2$, Kir3.1 (wild type or with TC tag ± RLuc), Kir3.2 and/or Kir3.2Luc (RLuc or NLuc). See Table 2 for transfection conditions. A full complement of heterotrimeric G proteins as well as receptor were transfected to maximize channel activation, and full functional complexes of receptor and channel were present to allow us to study both direct and indirect channel activation.

For electrophysiology experiments, 150 μl of HEK 293 T cells from a confluent T75 flask were plated in a 6 well plate the day before transfection. Each well was transfected with 1.55 μg of DNA using Lipofectamine 2000 as per the manufacturer's recommendations. Transfection conditions consisted of 1 μg m-Flag-δOR, 0.5 μg Kir3 channel and 0.05 μg Venus (as had been previously generated [9]). If a Kir3.1 construct was to be assessed, 0.25 μg of each the Kir3.1 and a Kir3.2 were transfected to allow correct processing and trafficking of Kir3.1 subunit-containing channels to the plasma membrane. The addition of the Venus construct was to aid in identifying transfected cells when performing electrophysiological recordings. 5 h post transfection, the media was changed to DMEM + 5% FBS in order to remove the transfection media to minimize cell toxicity.

2.5. Stable cell lines

HEK 293 cells were seeded at a density of 4.2×10^6 cells in 100 mm Petri dishes, cultured for 24 h, and transfected with 6 μg mouse-Flag-δOR, 5 μg Kir3.1-RLuc and 6 μg Kir3.2 using lipofectamine (Invitrogen). Two days post-transfection, cells were diluted and selected for using 500 μg/ml G418. Subsequently, colony outgrowths from single cell seeding were used to generate monoclonal cell lines. Receptor and channel subunits expression were then verified by western blot and electrophysiological recordings. Cells were grown and maintained in complete DMEM containing 10% (v/v) FBS, 1000 units/ml penicillin, 1 mg/ml streptomycin and 2 mM L-glutamine, in a humidified atmosphere of 5% CO^2 at 37 °C.

2.6. Electrophysiology

Twenty-four hours after transfection, the cells were trypsinized and resuspended in DMEM before plating on poly-D-lysine-coated 35-mm culture dishes. The following day, the cells were used for electrophysiological recordings. On the day the experiments were conducted, culture media were replaced with high-potassium solution (HK^+ external, 5 mM NaCl, 140 mM KCl, 2 mM $CaCl_2$, 1 mM $MgCl_2$, 20 mM HEPES, 10 mM glucose pH 7.4, 300 mOsmol/l). The plate was placed on the microscope stage, and the cells were perfused with HK external by a large-volume, gravity-fed perfusion system until seal formation began. Patch pipettes were pulled from borosilicate glass, and when filled with a HK ATP/GTP-containing solution (140 mM KCl, 20 mM NaCl, 5 mM EGTA, 5.4 mM $MgCl_2$, 10 mM HEPES, 2.5 mM K_2ATP, 0.3 mM Li_2GTP), they had an internal resistance between 2 and 5 MΩ. Cells were patched in the whole-cell configuration and voltage clamped with 85% compensation for series resistance using an Axopatch 200B and ensuring that cell capacitance was <30 pF. Cells were then subjected to a ramp protocol, which clamps the membrane potential from −100 to +50 mV at a rate of 1 mV/ms using Clampex 10.2 software. The ramping protocol was then repeated every 250 ms for 75 s. Agonists were suspended in HK external (1 μM final) and applied to the cell by a small-volume gravity-fed perfusion system directly next to the patched cell. Once peak current was observed, agonists were washed out of the bath by perfusing HK external from a large-volume gravity-fed perfusion system. Trace data were presented by plotting the current at −100 mV during the ramp protocol against time using Clampfit 10.2. Data were collected with a low-pass Bessel filter at 5 kHz and digitized with a Digidata 1440A.

2.7. FlAsH labeling of the TC-domain

On the day of experiment, transfected cells were washed once in wash buffer (HBSS, 1 mM $CaCl_2$, 490 μM $MgCl_2$, 0.1% D-glucose), before incubation for 1 h in labeling mix (HBSS, 1 mM $CaCl_2$, 490 μM $MgCl_2$, 0.1% D-glucose, 1.25 μM FlAsH-EDT_2 (Life Technologies), 250 nM 1,2-ethanediothol at 37 °C.[2] Cells were labeled in minimal labeling mix[3] (2–3 ml per 100 mm plate to ensure cells were covered). Post labeling, cells were washed twice in wash buffer (HBSS, 1 mM $CaCl_2$, 490 μM $MgCl_2$, 0.1% D-glucose,

[2] *Technical Tip:* To ensure for specific binding of the FlAsH-EDT_2 to the TC domain that was introduced into the proteins of interest, we included 250 nM EDT in the labeling mix to compete for the FlAsH-EDT_2 for non-specific binding sites. Post labeling, we washed with 250 μM BAL, which has been shown to be efficient at binding to free FlAsH-EDT_2, thereby removing any background FlAsH-EDT_2 labeling [10].

[3] *Technical Tip:* Use of the minimal volume of labeling media to cover cells and to ensure their health is necessary, as we want to minimize the amount of FlAsH-EDT_2 used for each plate, due to cost constraints. FlAsH-EDT_2 is an expensive reagent.

Table 2
DNA amounts of Kir-3.2-donor/TC-Kir3.1 acceptor pairings transfected in HEK-293 cells, together with m-Flag-δOR and complementary Gαβγ subunits.

	BRET assay biosensors[a]							
	Biosensor pair	Kir3.1 (TC)	Kir3.2	Kir3.2-Luc	$G\alpha_0$	$G\beta_1$	$G\gamma_2$	m-Flag-δOR
Intra-molecular	Kir3.1-TC-RLuc	10	10	0	1	1	1	4
Inter-molecular	Kir3.2-RLuc/Kir3.1-TC	10	7	3	1	1	1	4
	Kir3.2-NLuc/Kir3.1-TC	8	6	2	1	1	1	4

	Electrophysiology[b]				
		Kir3.1 (TC)	Kir3.2	m-Flag-δOR	Venus
Whole cell patch-clamp	Kir3.1 constructs	0.25	0.25	1	0.05
	Kir3.2 Constructs	0	0.5	1	0.05

[a] All values are in μg/100 mm plate.
[b] All values are in μg/35 mm plate.

250 μM 2,3-dimercapto-1-propanol (BAL) for 10 min each wash, at 37 °C. Cells were then suspended in Tyrode's solution (140 mM NaCl, 2.7 mM KCl, 1 mM $CaCl_2$, 12 mM $NaHCO_3$, 5.6 mM D-glucose, 490 μM $MgCl_2$, 370 μM NaH_2PO_4, 25 mM HEPES), before being plated into a 96-well plate for BRET assays. Cells were distributed in the 96-well plates to have a final protein concentration of between 5 and 1.5 μg/ml, in a 100 μl final volume per well.

2.8. Immunohistochemistry

Cells were plated onto coverslips pretreated with poly-L-lysine hydrobromide, and then transfected as described above. On the day of experiment, live cells were incubated with primary antibody for m-Flag-δOR (anti-Flag M1 antibody) (1/200 dilution) in DMEM media, thereby marking the receptor present at the plasma membrane.

Post exposure to Flag antibody, cells were washed in PBS-CM (2.7 mM KCl, 137 mM NaCl, 8 mM Na_2HPO_4, 1.5 mM KH_2PO_4, 1 mM $MgCl_2$, 1 mM $CaCl_2$) before being fixed in PBS-4% paraformaldehyde. After 20 min at 37 °C, cells were and rinsed with PBS-CM, then permeabilized with PBS-CM + Triton X-100 0.1% for 20 min at RT. A second wave of primary antibodies, this time on the fixed and permeabilized cells allowed us to stain for Kir3.1 (1/500 dilution) to label Kir3.1-TC constructs. Cells were again washed in PBS-CM, and subsequently blocked (PBS-CM, 1% BSA, 0.1% Triton X-100) for 10 min at RT before being incubated with Alexa-Fluor secondary antibodies (1/1000 dilutions for all) in PBS-CM (0.5% BSA, 5% goat serum, 0.1% Triton X-100) for 1 h, at room temperature, in the dark. Before mounting, the coverslips were washed in PBS-CM and mounted on slides with Immu-Mount (Thermo Scientific). Images were captured using a Leica LSM510 microscope (Leica, Wetzlar Germany), and these images were processed with LSM Image browser (Leica).

2.9. BRET measurements

96-well plates were loaded with FlAsH-labeled cells as prepared above (Section 2.6), and stored at 37 °C in the incubator until required.

5 min before BRET measurements were taken, plates were recovered from the incubator and h coelenterazine (NanoLight Technology) was added to each well (0.1 μg/100 μl in well). For both single point measurements, as well as the dose–response curves, 2 min before BRET readings, drugs of interest were manually added.[4] This delay was imposed by manual completion of the assays implied ~30% decay in the peak signal. To avoid confounding from this factor measures were systematically taken 2 min after drug exposure.

Readings were taken at 37 °C or room temperature, with a Mithras LB 940 plate reader (Berthold Technologies, Germany),[5] which allowed sequential integration of signals detected in the 440–480-nm (RLuc/NLuc emission) and 520–550-nm (YFP/FlAsH emission). BRET was expressed as the ratio of light emitted by fluorescence (measured at 530 nm) over the light emitted by RLuc (measured at 485 nm). Both luminescence and fluorescence were measured for 0.5 s for each read.

For total fluorescence readings, the readings were also taken at 0.5 s, at 535 nM, with excitation by laser at 485 nm. For total luminescence, where mentioned, the luminescence from the BRET reading was used.

To calculate net BRET, we took the BRET signal generated by donor constructs in cells where no TC domain was present, and subtracted this value from the BRET ratio generated by each of our Luc:TC-FlAsH biosensor pairings, thereby obtaining the specific energy transfer produced by each pair of constructs.

To calculate agonist-induced BRET (ΔBRET), we subtracted net BRET values for each of the control, or non-stimulated conditions from net BRET values corresponding to the stimulated condition.

2.10. FluXor assays of channel activity

Assays of channel activation were carried out using the Fluxor system (Invitrogen) as per manufacturer's instructions. Stable cells (Section 2.5) were seeded into a 96-well plate, at a density of 150 K cells per well, and left for 48 h. On the day of the experiment, cells were washed once with PBS, and incubated in 50 μl of Loading Buffer for 1 h at room temperature in the dark. The Loading Buffer was removed, and exchanged for Assay buffer, in which the cells were kept, at room temperature, in the dark, until required. Drugs were diluted in Stimulus Buffer, and fluorescence readings were taken after 5 min with the Mithras Plate reader at 535 nM.

2.11. Statistical analysis

Statistical analysis was carried out using the Graphpad 5 software package as detailed in corresponding figure legends.

3. Results

3.1. Biosensor design

The overall goal of this study was to provide proof of principle that biosensors which capture conformational changes undergone

[4] *Technical Tip:* For the use of DMSO and NH_4OH with drug dilutions, see Supplementary Fig. 4.

[5] *Technical Tip:* A Victor Plate reader (PerkinElmer Life Sciences, Waltham, MA) was used for optimization of transfection and labeling conditions using the TC-RLuc construct. However the greater sensitivity of the Mithras meant that it was used for all other experiments, as it alone could allow for the measurement of the small conformational changes monitored by these biosensors.

by channel proteins constitute a valid approach to identify drugs that influence channel function. To do we developed biosensors for Kir3 (GIRK) channels, a choice that was based on several considerations. First, Kir3 channel modulators have potential therapeutic application in various areas including pain perception, anxiety and arrhythmias [11–14]. Second, the K^+ selectivity filter and the topology of the subunits that define the ion path is conserved across channels of increasing complexity, including voltage-gated kV channels [15], suggesting that the biosensors developed for Kir3 channels could be eventually used as templates for other related family members. Third, Kir3 channel subunits have only two transmembrane spanning domains, making them simple to express in heterologous systems and manipulate by molecular biology techniques. Fourth, Kir3 channel opening does not require changes in membrane voltage, allowing us to work with a simple experimental set-up.

The ability to insert donor/acceptor BRET pairs without losing channel functionality was inherent in the ability to optimize the proposed biosensors. Thus, tag size for resonance energy transfer had to be taken into account. Traditional BRET tags are large and bulky which in most cases restricts their location to N- and C-terminal domains of proteins. The *Renilla*-Luciferase (RLuc) itself, which has long been used as a source of luminescence in BRET is 36 KDa [16]. However, recent advances in protein engineering have made smaller epitopes like Nano-Luciferase® (NLuc; 19 kDa) available which also gives a more powerful luminescence signal upon contact with the coelenterazine substrate [17]. Both donor systems were tested in BRET pairs where the acceptor was the fluorescin derivative, fluorescin arsenical hairpin binder-ethanedithiol (FlAsH-EDT_2). Non-fluorescent in its native state, FlAsH-EDT_2 emission occurs when it binds to a tetracysteine (TC) (CCXXCC) motif in the protein of interest [10,18]. The most common motif and one that has been previously validated as BRET acceptor [6], consists of a chain of six residues (Cys-Cys-Pro-Gly-Cys-Cys) that were introduced at different positions within Kir3 channel subunits.

Donor acceptor BRET pairs were introduced into channel subunits so as to produce two types of biosensors: (a) *inter-molecular biosensors* where the donor (RLuc or NLuc) was located in one subunit of the Kir3.1/Kir3.2 heteromer and the TC-FlAsH-binding domain in the other, or (b) *intra-molecular biosensors* in which both donor and acceptor moieties were bio-engineered into the same subunit. In the latter, the donor was always RLuc and was consistently placed at the C-terminus of Kir3.1 subunits. On the other hand, the TC-domain for the FlAsH acceptor was alternatively located at the N-terminus (NT-TC), several residues downstream of this position (N20-TC; N70-TC) or in cytosolic loops (βBβC; βGβH) of the C-terminal domain (Fig. 1). For inter-molecular biosensors acceptors were kept at these same locations but the donors, alternatively RLuc or NLuc, were located at the C-terminal end of Kir3.2. The different donor acceptor constructs produced in the study and their combination into BRET pairs is summarized in Table 1.

The choice for the different locations of the TC-domain was guided by crystallography studies of Kir3.2 [19] and KirBac [20], which have recently revealed the type of movements that may take place as the channel interconverts between active and inactive states. TC-domains were introduced in conservative manner, always protecting regions associated channel activation even if it meant capturing smaller displacements. Among BRET pairings tested in the *inter-molecular* format those bearing Kir3.2 donors and NTD acceptors were designed to capture rotational movements of the CTDs. Those bearing acceptors in cytosolic loops were expected to report on dilation–constriction movements by monitoring changes in distance between the loops in one subunit and the C-terminus of the neighboring one. *Intra-molecular biosensors* in which the donor was fixed at the Kir3.1 C-terminus and acceptors located at the NTD were designed to monitor rearrangements that occur during activation in which NTDs tend to approach the CTD of the same subunit. The TC-domain separately engineered into alternate sites along cytosolic loops βB-βC and βG-βH were expected to be most affected by the apposition of the Gβγ subunit onto βL-βM and βD-βE sheets respectively above each of these acceptor locations.

3.2. Verification of construct localization and function

After the constructs for the different insertions of the tetra-cysteine (TC) domain, were generated, validation of each was carried out with respect to two criteria: their expression at the membrane and the ability to pass current. Of course, expression at the plasma membrane is necessary if the channel can conduct a current as measured using patch clamp, however, we validated both these outcomes, by electrophysiology and using immunohistochemistry. This latter approach also allowed us to control whether Kir3.1 constructs reached the plasma membrane. Specifically, if the Kir3.1 subunit is present at the surface, it follows that Kir3.2 is also there. Indeed, since Kir3.2 is necessary for plasma membrane targeting of Kir3.1 the only way the latter can be expressed at the surface is in a heteromer with Kir3.2 [21].

To assess channel functionality the different TC-tagged constructs were heterologously expressed in HEK 293T cells. Individual cells were patch clamped in the whole cell configuration and current was recorded using a voltage clamp protocol in response to GPCR stimulation. Each construct was transfected in the presence of the δOR, a receptor known to activate Kir3 channels, and channel functionality was assessed by stimulation of the receptor with the agonist DPDPE (Fig. 2A and Supplementary Fig. 1) [22]. Cells transfected with the different TC-tagged constructs were able to respond to δOR stimulation to varying degrees. It should be noted that the recorded currents were not normalized to the expression level of the channel at the cell surface and therefore may explain variability in peak currents. Upon washout of the agonist from the cell bathing solution, a return of the current to pre-agonist stimulation levels was noted for all the constructs tested.

Immunohistochemistry experiments were carried so as to qualitatively assess surface expression of Kir3.1 subunits whether they were integral part of intramolecular biosensors (Fig. 2C – i) or as part of the acceptor construct in intermolecular pairings (Fig. 2C – ii). Thus, to visualize its subcellular distribution, an antibody which recognized an epitope in the CTD of the Kir3.1 subunit was used. As shown in both figures, although part of the overexpressed subunit remained intracellular, a considerable amount of Kir3.1 (brought to the surface via interaction with Kir3.2) made it to the plasma membrane. This is evidenced by colocalization of Kir3.1 immunoreactivity with Flag-δORs that were specifically labeled at the plasma membrane.

A final means of verification of the presence of the δOR-Kir3 biosensor at the plasma membrane was through use of non-membrane permeable peptide agonists, to obtain a BRET response. As detailed in following sections, peptidic agonists like DPDPE or deltorphin B were able to induce BRET changes, corroborating plasma membrane expression of the tested BRET pairs.

3.3. Optimization of FlAsH-EDT_2 labeling conditions

The optimal conditions for transfecting and labeling cells with FlAsH-EDT_2 were then determined for HEK 293 cells expressing the TC-RLuc construct (4 μg and 10 μg/100 mm dish, see Section 2.2.4), a chimeric tool designed to easily measure FlAsH-EDT_2-luciferase-based BRET, thereby allowing us to

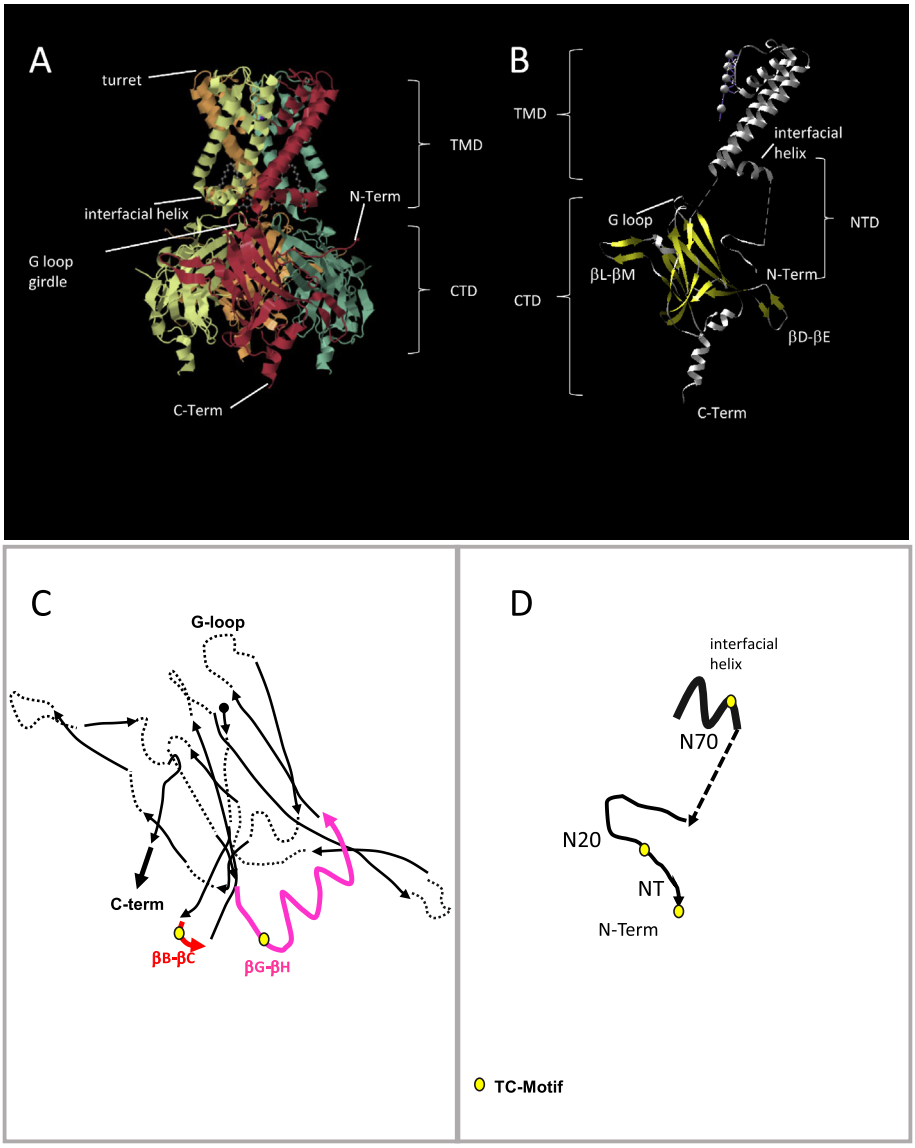

Fig. 1. Schematic representation of Kir3 channel and sites of tag insertion. (A) 3D representation of structure of tetrameric Kir3 channel as formed by four Kir3.2 subunits (http://www.rcsb.org) shows the pore forming transmembrane domain (TMD) as well as the intra-cellular N-terminal domain (NTD) and C-terminal domain (CTD). (B) Single subunit of Kir3 channel, showing TMD and CTD, and their location with respect to the NTD of the same subunit. (C) Line diagram of the CTD of Kir3, where solid lines are beta-sheet, and the dotted lines are intra-beta-sheet loops. In color are the two inter beta-sheet loops that were chosen for insertion of TC tag. (D) Line diagram concentrating on the N-terminal domain and interfacial helix, showing the relative locations of the N-terminally inserted TC tags (NT, N20 and N70).

determine the minimal amount of the TC domain necessary for labeling, and the amount of FlAsH-EDT$_2$ label which yielded a strong and specific BRET signal in our system. The supplier's suggested concentration for labeling was 2.5 μM, whereas it has previously been shown that 500 nM may also yield sufficient labeling strength for fluorescence to be measured in intact cells [10]. To ensure the optimal FlAsH-EDT$_2$ concentration to measure fluorescence and BRET-induced fluorescence in live cells, we tested 250 nM, 500 nM, 1.25 μM and 2.5 μM of the fluorescent label (Fig. 3A and C). By comparing Fig. 3A and B to C and D we concluded that only cells transfected with the higher amount of DNA were specifically labeled (Fig. 3A vs C) generating a measurable, specific net BRET signal (Fig. 3B vs D). Moreover, titration of FlAsH-EDT$_2$ concentration showed that although 2.5 μM allowed for maximal fluorescent output and net BRET, labeling with 1.25 μM was equally strong and reproducible, and 1.25 μM FlAsH-EDT$_2$ was therefore chosen for future experiments.

3.4. Expression of Kir3 channel constructs and stoichiometry of channel subunits

Three factors need to be taken into account for optimal expression of Kir3 BRET pairs at the plasma membrane. First, we need a sufficiently high amount of TC domain expression to warrant a BRET signal over the background. Second, the stoichiometry of the Kir3.1 vs Kir3.2 channel subunits should ensure Kir3.1 expression at the membrane, and finally the BRET donor:acceptor ratio must be considered. This latter aspect only applies to the inter-molecular biosensor pairs.

Based on observations of the TC-RLuc donor–acceptor construct, 10 μg/100 mm dish of DNA of TC domain-containing proteins was required for specific RLuc:TC-FlAsH energy transfer. With this in mind, we used 10 μg of TC-Kir3.1-RLuc in our intra-molecular BRET biosensors, and 10 μg of TC-Kir3.1 transfected in parallel with the Kir3.2-RLuc for inter-molecular pairings.

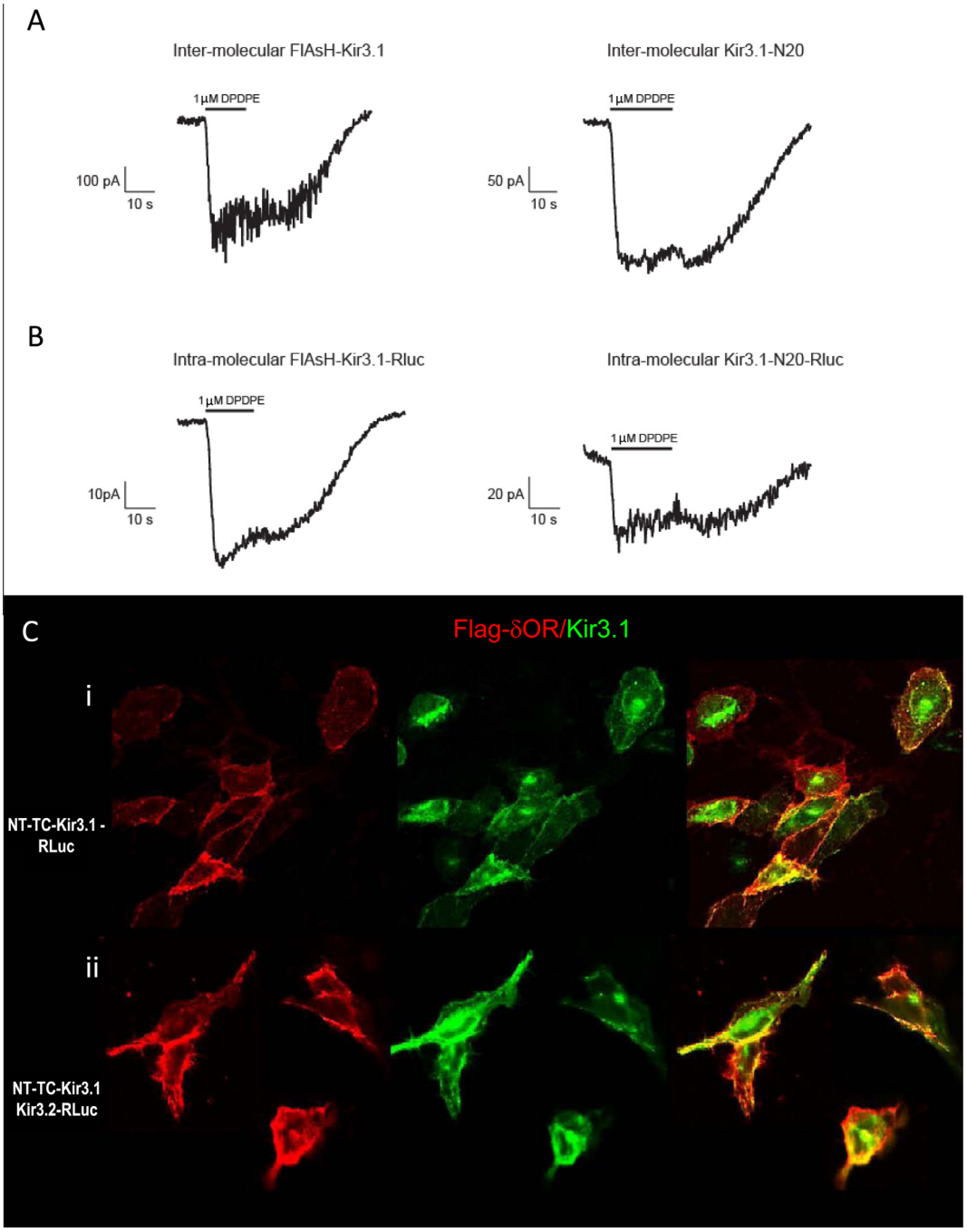

Fig. 2. Validation of electrophysiological competence and membrane expression of intermolecular and intramolecular Kir3.2-RLuc/Kir3.1-TC constructs. (A) Inter- and (B) intra-molecular NT and N20 TC tagged Kir3.1 constructs conduct current following activation with the δOR agonist DPDPE. HEK 293 cells transfected with the sensor construct, WT Kir3.2 and δORs were patch clamped in the whole cell configuration in a bath containing high K^+ concentration (as detailed in Section 2). Patched cells were treated with 1 μM DPDPE diluted in HK solution. Current traces shown were normalized to cell capacitance (pA/pF) and were sampled at a rate of 4 Hz. Membrane expression of NT-TC-Kir3.1 constructs in (C) inter- and (D) intra-molecular pairs. HEK 293 cells were transfected with Flag-δORs, the indicated BRET pairs together with complementary channel and $G\alpha_o\beta_1\gamma_2$ subunits. The day of the experiment, cells were incubated with anti-Flag antibody to specifically label Flag-δORs expressed at the membrane (red). Cells were then fixed and permeabilized before incubation with an antibody that specifically recognizes the CTD of Kir3.1 subunits (green). Fluorescent second antibodies were then used to reveal each species using confocal microscopy. Note co-localization of the channel protein with δORs labeled at the membrane. Traces correspond to a single experiment.

An additional concern for optimal expression of Kir3 channels is the ratio of transfected Kir3.1:Kir3.2 subunits. Kir3.1 alone cannot form a channel alone as it is retained in the endoplasmic reticulum [23,24], requiring Kir3.2 or other Kir3 subunits to traffic to the plasma membrane [25]. The exact stoichiometry by which Kir3.1/Kir3.2 heteromers transit to the membrane is unknown. However in our hands, we found that a 1:1 Kir3.1:Kir3.2 transfection ratio allowed monitoring BRET changes induced by peptidic ligands, which suggested adequate amounts of the TC-Kir3.1 acceptor construct were delivered to the cell surface.

For the Kir3.1-TC-RLuc constructs, expression at the plasma membrane was a simple matter of transfecting equal amounts of tagged Kir3.1 and untagged Kir3.2 subunits. However, with both our inter-molecular BRET pairs (Kir3.2-RLuc and Kir3.2-NLuc), we did not want to over express the luciferase component of the BRET pair, since readings are usually taken at 'saturation', which

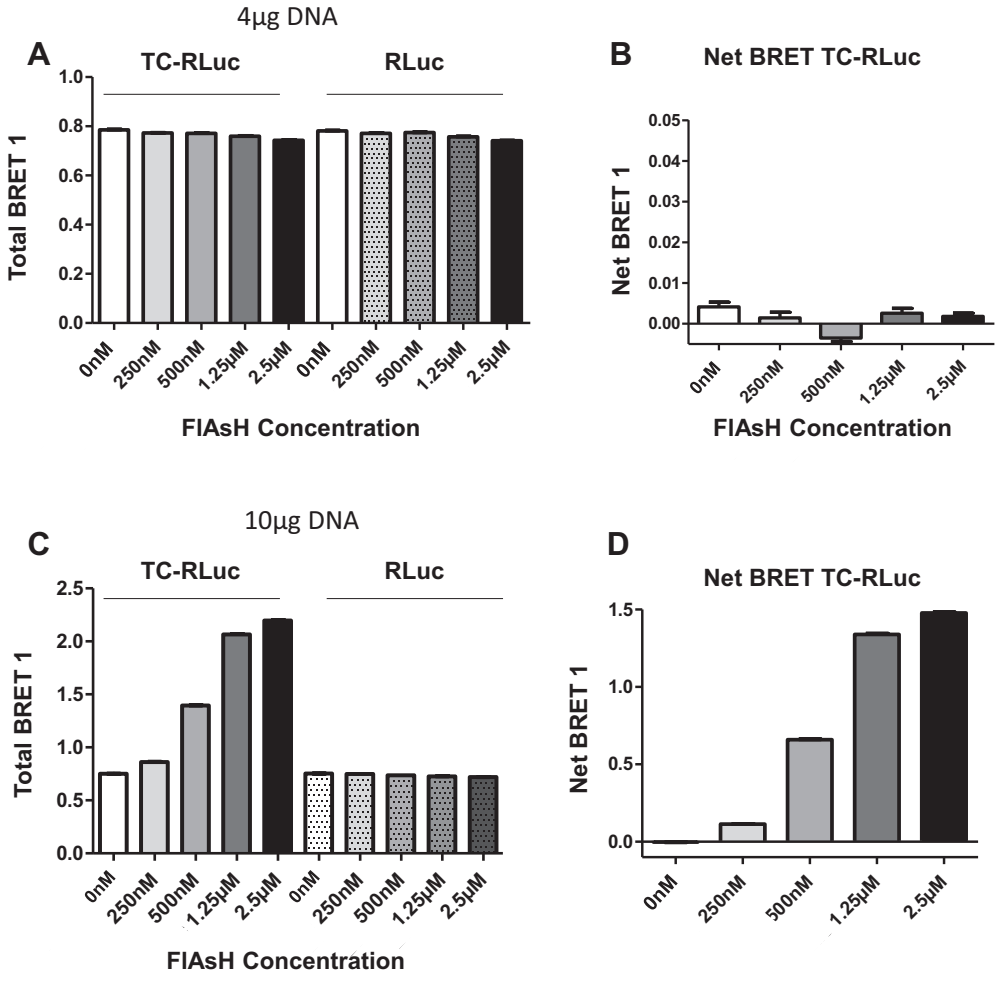

Fig. 3. Optimization of FlAsH-EDT$_2$ labeling for BRET assays. A TC-RLuc fusion protein was used to determine optimal labeling and transfection conditions to obtain adequate transfer of energy between RLuc donor and FlAsH acceptor. HEK 293 cells were transfected with 4 µg (A and B) and 10 µg (C and D) of TC-RLuc construct or with RLuc by itself, and incubated with increasing concentrations of FlAsH-EDT$_2$ as indicated. The total BRET signal in cells transfected with 4 µg of TC-RLuc was not greater than the background signal obtained with RLuc alone (A) and net BRET was therefore not detected (B). In cells transfected with 10 µg of TC-RLuc construct, BRET increased in proportion with the concentration of FlAsH-EDT$_2$ added to the medium but not in cells transfected only with RLuc (C). Here, net BRET was proportional to FlAsH labeling concentrations (D). Data correspond to one labeling test carried out in triplicate (error bars contained within bar outlines).

corresponds to a situation where theoretically every donor is matched with an acceptor moiety [26]. Matching is not a concern with the intra-molecular biosensor pairings, as there was an inbuilt 1:1 ratio, which could not be changed, but was an issue that had to be resolved for the inter-molecular biosensor pairings.

To address this latter issue, we tested various ratios of Kir3.1-TC:Kir3.2-Luc:Kir3.2wt (data not shown), to see which ensured integration of the channel into the membrane, while still allowing for a robust BRET signal. These tests were carried out as mentioned in Section 3.2, by comparing responses to membrane-permeable and non-permeable δOR agonists. Thus for intermolecular pairs, we maintained the amount of TC-Kir3.1 construct and tested different combinations of Kir3.2-RLuc/Kir3.2 untagged, maintaining the total amount of Kir3.2 subunit transfected equal to that of Kir3.1. Kir3.2-RLuc was reduced from 6 µg/100 mm petri, down to 0.5 µg, and untagged Kir3.2 was increased accordingly. Optimal BRET ratios were observed at Kir3.2-RLuc levels of 2–3 µg/100 mm dish.

Our initial trials showed that 10 µg/100 mm petri of the TC-RLuc control construct yielded a robust BRET signal. However, in addition to the channel a GPCR (which in this case was δORs) and complementary heterotrimeric Gαβγ subunits were also required to induce channel conformational changes associated with physiological activation of the receptor. Thus, δOR was included at a level previously shown to elicit Kir3 responses in HEK 293 cells (4 µg/100 mm petri) [8], as well as $G\alpha_o$ (1 µg), β_1 (1 µg) and γ_2 (1 µg), which are required not only to ensure channel activation *per se* but also to warrant proper assembly and trafficking of the Kir3 signaling complex [27]. Table 2 shows the amounts of DNA transfected per 100 mm dish for different biosensors and signaling partners. The stoichiometry of classical BRET pairs is usually given in terms of luminescence and fluorescence counts. In this case we opted for DNA ratios because non-transfected FlAsH labeled cells displayed high levels of background fluorescence. In spite of this background specific BRET signals can be monitored [6,28].

3.5. Basal net BRET readings elicited by Kir3.1-TC constructs using Renilla luciferase as donor

Once the optimal transfection conditions were established, we measured basal net BRET in each of our intra-molecular constructs, as well as in inter-molecular BRET pairings with Kir3.2-RLuc. When working with the TC-RLuc construct, we obtained a net BRET value approximately equal to 1 (Fig. 3D). This is most probably due to a combination of factors including: (a) donor and acceptor stoichiometry being 1:1, (b) donor/acceptor moieties being kept close

together by a small linker [6] and (c) possible bystander BRET due to overexpression of such a small linear construct which would allow energy transfer not only within but among neighboring constructs. When the RLuc and TC-domain were transferred into channel subunits, whether the intra- or inter-molecular pairings, much of this energy transfer was lost, most likely because of an increase in the distance between donor/acceptor pairs and loss of bystander BRET. Thus, net BRET values for the RLuc-based biosensors was reduced considerably as compared to the TC-RLuc construct (Fig. 4A).

Both intra- and inter-molecular biosensors yielded stable net BRET values and, when compared in terms of these values, the former displayed higher basal energy transfer than the latter (Fig. 4A). This could be explained because luminophore and fluorophore are correspondingly located on the same or different Kir3.1 subunits, or because less Kir-3.2-RLuc was transfected for inter-molecular sensors. Moreover, independent of whether w intra- or intermolecular, constructs bearing the TC domain in cytosolic loops were always less well expressed than those labeled within the NTD (not shown), suggesting that these cytosolic loop are essential for expression or stability. These differences prevented us from comparing these two groups any further. On the other hand, expression levels of Kir3.2-RLuc/NT-TC-Kir3.1 and Kir3.2-RLuc/N20-TC-Kir3.1 were not different from one another, and neither was the expression of NT-TC-Kir3.1/RLuc and N20-TC-Kir3.1-RLuc. This allowed us to infer that even a change in relative position as small as 20 residues could be detected (Fig. 4A), speaking to the sensitivity of the BRET/FlAsH approach.

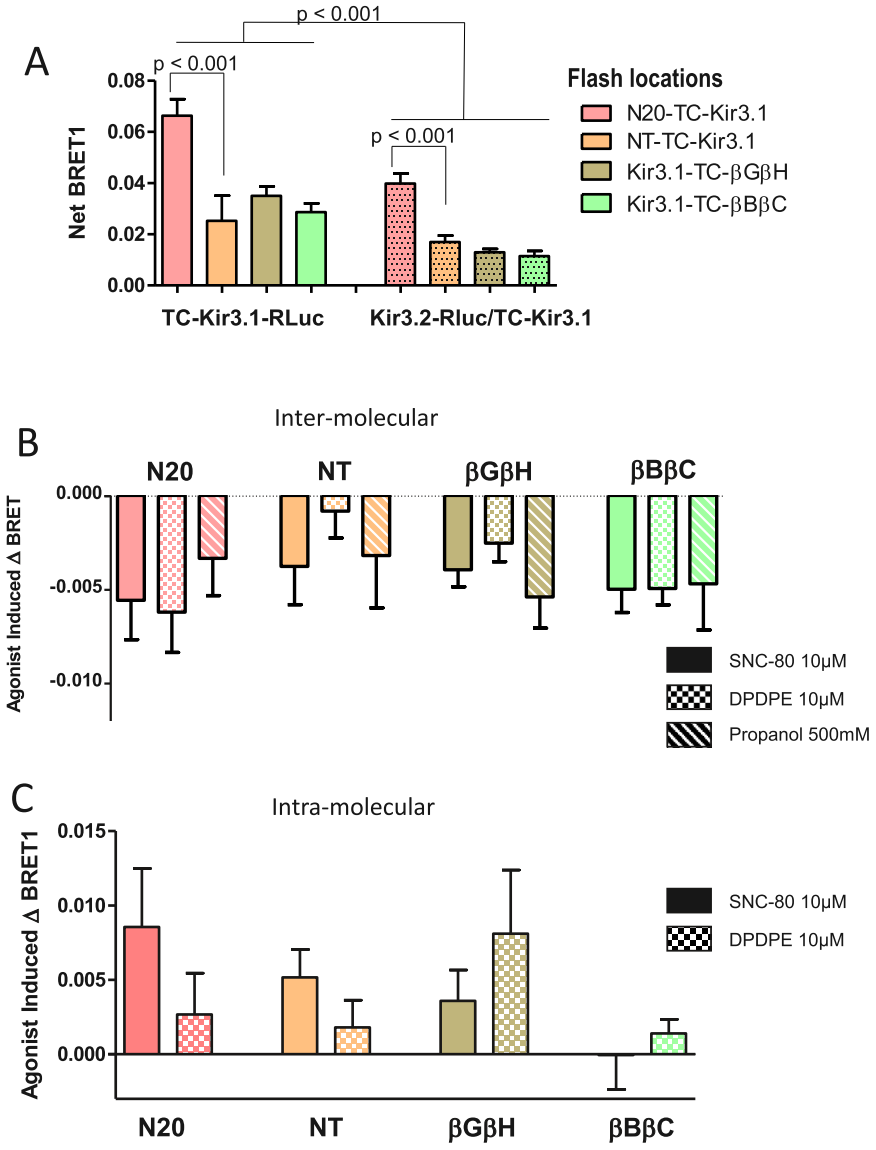

Fig. 4. Characterization of BRET signals generated by intermolecular and intramolecular RLuc BRET pairs. (A) Basal net BRET was monitored in HEK 293 cells expressing δORs, the indicated constructs together with complementary $G\alpha_o\beta_1\gamma_2$ and untagged Kir3.1/Kir3.2 channel subunits. Data represent mean net BRET ± SEM and correspond to 5–11 independent experiments. Results were analyzed using two way ANOVA which showed an effect of donor location ($p < 0.001$), of acceptor location ($p < 0.001$) and an interaction ($p < 0.001$). Post-hoc analyses indicated a significant effect of donor location within each set of biosensors as shown in the figure. Cells were transfected as in (A) to express different types of (B) intermolecular or (C) intramolecular biosensors and exposed to the indicated agonists. Data are expressed as mean agonist-induced change in BRET (ΔBRET ± SEM) and correspond to 3–9 independent experiments carried out in triplicate. Each set of data was independently analyzed using two way ANOVA on the corresponding net BRET values. No significant ligand effects were observed nor an effect of TC-domain location within each group of biosensors. Two way ANOVA was used to compare SNC-80 and DPDPE-induced BRET changes at each corresponding intramolecular and intermolecular pair. For all biosensors, except βBβC, there was a significant effect of the vantage point from which drug effect were monitored ($p < 0.05$), no effect of drug and no interaction.

Please cite this article in press as: D.N. Robertson et al., Methods (2015), http://dx.doi.org/10.1016/j.ymeth.2015.07.011

3.6. Agonist-induced changes in energy transfer for BRET biosensors containing Renilla luciferase as a donor

We next assessed if RET could be modulated by channel activation. Channel activation can be achieved in two ways either through direct activation using channel ligands such as propanol [29] and ML-297 [30] or via stimulation of receptors that physiologically control their activity, such as the δ-opioid receptor (δOR) [22]. We first monitored changes in the inter-molecular biosensors expressed in HEK 293 cells together with δORs as well as the G protein heterotrimer $G\alpha_o\beta_1\gamma_2$. We observed that for all TC-domain positions in the Kir3.1 subunit, δOR activation either with a peptidic agonist DPDPE, (10 μM, 5 min), or the non-peptidic agonist SNC-80 (10 μM, 2 min) caused a small and variable decrease in RET that did not reach statistical significance for any of the BRET pairs tested (Fig. 4B). To determine whether this minimal effect was due to inefficient channel activation by δOR, we also assessed BRET induced by propanol, an alcohol that directly binds and activates these channels [29]. BRET changes induced by the direct ligand were not larger and remained equally variable as those induced by receptor activation.

Activation-induced BRET changes were also monitored with intra-molecular biosensors (Fig. 4C), but the overall outcome was similar to that observed with intra-molecular constructs. However, an encouraging observation was that intra and inter-molecular biosensors displayed opposing changes in energy transfer upon activation (compare Fig. 4B and C). These differences were indeed significant for all pairs of biosensors, except those bearing the TC-domain in the βBβC loop. Such opposing changes in the directionality of BRET are consistent with the notion that acceptor tags are moving in distinct ways whether donor/acceptor moieties are located in the same or in adjacent channel subunits.

In summary, despite the presence of stable basal BRET distinctively modified in intra vs inter-molecular constructs, the magnitude of the net BRET signal was low and changes invoked by channel activation were not significant. It was therefore necessary to improve the dynamic window in order to produce viable biosensors.

3.7. Improving RET and dynamic window of Kir3.1 channel biosensors

The data obtained with intra vs inter-molecular TC/RLuc constructs was quite encouraging, from the point of view of allowing us to capture distinct activation-related conformational changes depending on whether donor and acceptor were on the same or different subunits. However, the problem of low net BRET signal and small dynamic window needed to be improved. To do so, two additional strategies were developed: (i) modification of the donor moiety to improve luminescent yield and subsequent RET, and (ii) exploration of additional positions of the TC-domain BRET acceptor within the Kir3.1 subunit.

3.7.1. The use of Nano-Luciferase as a BRET donor

RLuc had been previously modified to RLucII (or alternatively RLuc2 or RLuc8) in order to increase luminescence yield for short-lived emissions produced by the substrate Deep-Blue coelenterazine (DBC®) [31]. However, RLucII is also a 36 kDa protein, so we turned our attentions to a novel luciferase Nano-Luciferase that has also been engineered to yield stronger and more durable luminescence at wavelengths compatible with the TC-FlAsH excitation (508 nm) [17]. At 19 kDa, it has a much smaller spatial footprint than the 36 kDa *Renilla* luciferase, and thus less likely to disrupt Kir3 function.

One issue with NLuc is the reagent supplied as the substrate (Nano-Glow), which necessitates that cells be lysed for access to NLuc (Section 2.8, manufacturer's protocol). This was not useful for measuring BRET in live cells, so we first determined whether CH would be a substrate for NLuc. To this end, tests of luminescence output with CH and NLuc were carried out, to determine luminescence yield and kinetics of the BRET signal measured under such conditions (Supplementary Fig. 2A). As previously observed for CH/RLuc [32], the luminescent signal stabilized after 5 min (Supplementary Fig. 2). Thus, NLuc was established as a competent donor (Supplementary Fig. 2B), provided BRET was always measured with the same delay following CH addition, to avoid confounds from signal decay.

3.7.2. Production and validation of donor Kir3.2 constructs tagged with NLuc

Kir3.2 subunits were tagged with NLuc at two different positions within the C-terminal domain. In the first construct, NLuc was introduced as a direct replacement for RLuc in Kir3.2. This allowed us to make direct comparisons between the two RLuc and NLuc versions of the biosensor. In the second new Kir3.2-NLuc construct, the last 43 amino acids of the CTD were removed, placing NLuc at amino-acid position 380. The rationale for this was the presumption that placing NLuc closer to the body of the channel core (Fig. 1) would allow greater RET, consequently allowing us to better capture ligand-induced conformational rearrangements from this vantage point. Donor constructs were then tested for electrophysiological competence, membrane expression and ability to support traditional energy transfer. Kir3.2-NLuc and Kir3.2-ΔNLuc were functional channels in response to δOR stimulation with DPDPE (Supplementary Fig. 1) and afforded adequate expression of the Kir3.1-TC pairing at the plasma membrane (Supplementary Fig. 3).

Before using Kir3.2-NLuc constructs to produce channel biosensors, we tested the ability of this different type of donor to evoke a traditional BRET signal using YFP as the acceptor. We had previously used the Kir3.1-Luc/YFP-$G\gamma_2$ pair, to show that δOR activation induced a conformational rearrangement at the interface of the Gβγ dimer and Kir3 channel subunits which resulted in increased energy transfer [8]. We used this same readout to determine whether one of the NLuc constructs (Kir3.2-Δ380NLuc) produced similar results as those previously observed. As shown in Fig. 5A, confirming the BRET competence of the NLuc/YFP pair, ligand-dependent activation of the δORs with the peptidic agonist deltorphin B induced a sigmoidal increase in RET between Kir3.2-ΔNLuc and YFP-$G\gamma_2$.

In a second series of verification steps, we ran parallel BRET experiments to compare basal and ligand-induced changes in BRET for Kir3.2-RLuc/YFP-$G\gamma_2$ and Kir3.2-NLuc/YFP-$G\gamma_2$ pairs. We noted that when the same conditions of transfection were used, NLuc was ≈8-fold more efficient at producing luminescence than RLuc (Fig. 5B), which lead to a concomitant ≈4-fold increase in fluorescence emitted by the novel BRET pair (Fig. 5C). For both the RLuc and NLuc constructs coupled with YFP, basal and agonist-induced BRET were then evaluated. Because the increase in luminescence yield by NLuc (Fig. 5B) was larger than the corresponding increase in fluorescence emitted by the acceptor YFP (Fig. 5C), net BRET values were smaller for the novel, than for the traditional Luc/YFP pair (Fig. 5D). Note that total fluorescence emitted by YFP as assessed by laser excitation (not via BRET) was similar in cells transfected with RLuc and NLuc ($\text{Tot-Fluo}_{\text{RLuc}}$: $1.8 \pm 0.1 \times 10^6$; $\text{Tot-Fluo}_{\text{NLuc}}$: $1.7 \pm 0.1 \times 10^6$) such that differences in net BRET values cannot be attributed to differential expression of the YFP acceptor. Inspection of BRET changes induced by peptidic (DPDPE, 10 μM, 5 min) and non-peptidic (SNC-80, 10 μM, 5 min) δOR agonists were similar for both donors but less variable for the NLuc pair than for the RLuc pair (Fig. 5E). Taken together these results indicate that NLuc in combination with h coelenterazine behaves as a competent BRET donor. Thus, Kir3.2NLuc

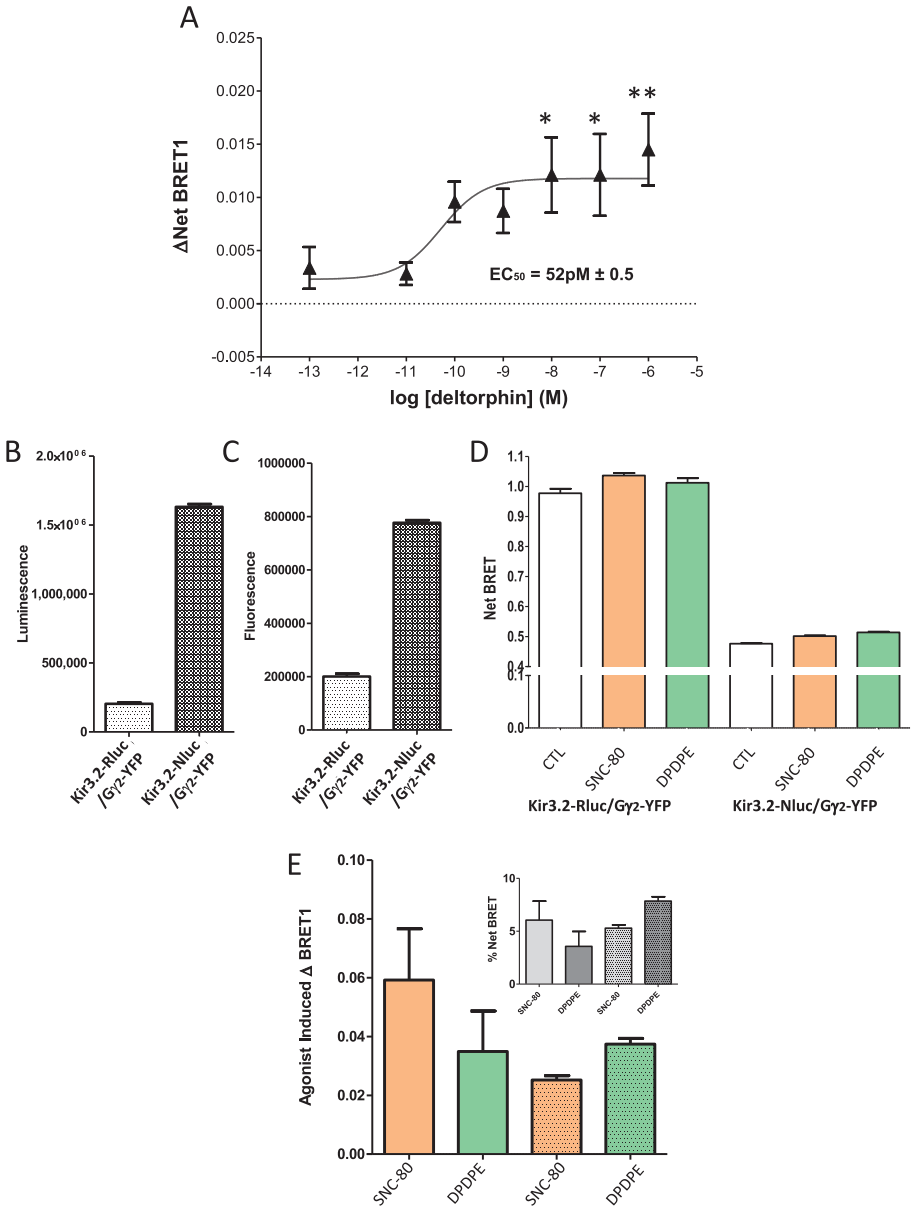

Fig. 5. Validation of NLuc as competent BRET donor. (A) HEK 293 cells transfected with δORs, the Kir3.2-ΔNluc/YFP-Gγ_2 pair and complementary Gα_o, Gβ_1 and untagged Kir3.1/Kir3.2 subunits were exposed to increasing concentrations of deltorphin B as indicated, and BRET measured 2 min after drug exposure. Data represent mean ΔBRET ± SEM of six independent experiments. They were analyzed by one way ANOVA ($p < 0.01$) and Dunnett post hoc test revealed an effect at higher concentrations as indicated in the figure. (B) Luminescence, (C) BRET-dependent fluorescence and (D) net BRET values were compared in cells transfected either with Kir3.2-RLuc or Kir3.2-ΔNLuc as indicated, together with YFP-Gγ_2 and complementary signaling partners as above. The day of the experiment, both groups of cells were exposed to the same concentration of h coelenterazine (0.1 μg/100 μl) and BRET measures taken in the presence or absence of the indicated ligands (10 μM; 10 min). (E) Histogram show agonist-induced changes in net BRET for these biosensor pairings. *Inset:* shows ligand-induced changes, expressed as a percentage of corresponding basal net BRET. Data shown in (B)–(E) correspond to mean ± SEM of triplicate readings, obtained in a single experiment run in parallel for the two donor systems.

constructs were co-expressed with Kir3.1-TC counterparts, and tested as a series of inter-molecular biosensors.

3.7.3. Production and validation of alternative acceptor TC-Kir3 constructs

In an effort to improve the dynamic window of our biosensors, we examined additional positions for the acceptor moiety, focusing on channel regions displaced upon activation but spatially distant from the Gβγ interaction interface. One such site is the interfacial helix [19], which undergoes a rotational movement that is correlated with permeability changes at the selectivity filter [20]. For this reason the TC domain was introduced at the start of the helix, 70 amino-acids downstream from the N-terminus of the Kir3.1 channel subunit (N70; Fig. 1A), and electrophysiological competence of the new construct was validated (Supplementary Fig. 2).

3.8. Intermolecular BRET biosensors with NLuc donor and FlAsH-TC acceptor

3.8.1. Basal and agonist-induced BRET by Kir3.1-NLuc/Kir3.1-FlAsH-TC biosensors

Having verified that NLuc is an efficient donor in classical BRET pairs, and having shown that Kir3.2-NLuc and Kir3.2-ΔNLuc were both electrophysiologically competent, we sought to determine if the NLuc donor could excite the FlAsH-TC acceptor in Kir3.1

subunits. For this purpose Kir3.2-NLuc constructs were first co-expressed with each of the Kir3.1 acceptors previously tested with RLuc. Fig. 6A shows a comparison of basal net BRET values obtained with NLuc/Kir3.1-TC and RLuc/Kir3.1-TC intermolecular biosensors. The only BRET pair in which the use of NLuc produced a sizable increase (~7-fold) in basal RET was NT-TC-Kir3.1, where the basal signal increased to 0.122 ± 0.003 in presence of NLuc as compared to 0.017 ± 0.004 measured with RLuc. (*Note:* the remaining 3 intermolecular NLuc pairs in the figure were not further pursued). Then the NT-TC-Kir3.1 donor was also tested with Kir3.2-ΔNLuc, with the expectation that a reduction in the distance between the C-terminal donor and the core of the channel would improve RET to Kir3.1-TC constructs labeled at the N terminus. This assumption was not confirmed, since basal net BRET at Kir3.2-ΔNLuc/NT-TC-Kir3 was not different from the value obtained with the full-length Kir3.2-NLuc subunit 1 (data not shown; observed basal net BRET for Kir3.2-ΔNLuc/NT-TC-Kir3: 0.112 ± 0.003).

After establishing that NLuc could excite FlAsH-TC on our previously characterized acceptor constructs, BRET generated by a new acceptor bearing the TC domain at the beginning of the interfacial helix (N70-TC-Kir3.1) was also tested. Basal energy transfer by the Kir3.2-NLuc/N70-TC-Kir3.1 pair was low (0.017 ± 0.004, Fig. 6B) but channel activation by deltorphin B (100 nM, 2 min) still produced a small, significant decrease in the signal (−0.005 ± 0.0004, Fig. 6C). In an effort to improve transfer, we tested the new acceptor construct N70-TC-Kir3.1 with two different donor combinations. First, we assessed whether the use of the truncated Kir3.2-ΔNLuc donor could be beneficial but this was not the case (0.021 ± 0.005, Fig. 6B). In a second and final attempt we explored whether using N70-TC-Kir3.1 with a combination of two donors, one in the intramolecular position and the other in intermolecular location would improve low energy transfer. Thus, the donor RLuc was introduced at the C-terminus of N70-TC-Kir3.1 to yield N70-TC-Kir3.1-RLuc. This intramolecular pair in its own displayed a net BRET value of 0.07 ± 0.003 but no response to deltorphin B

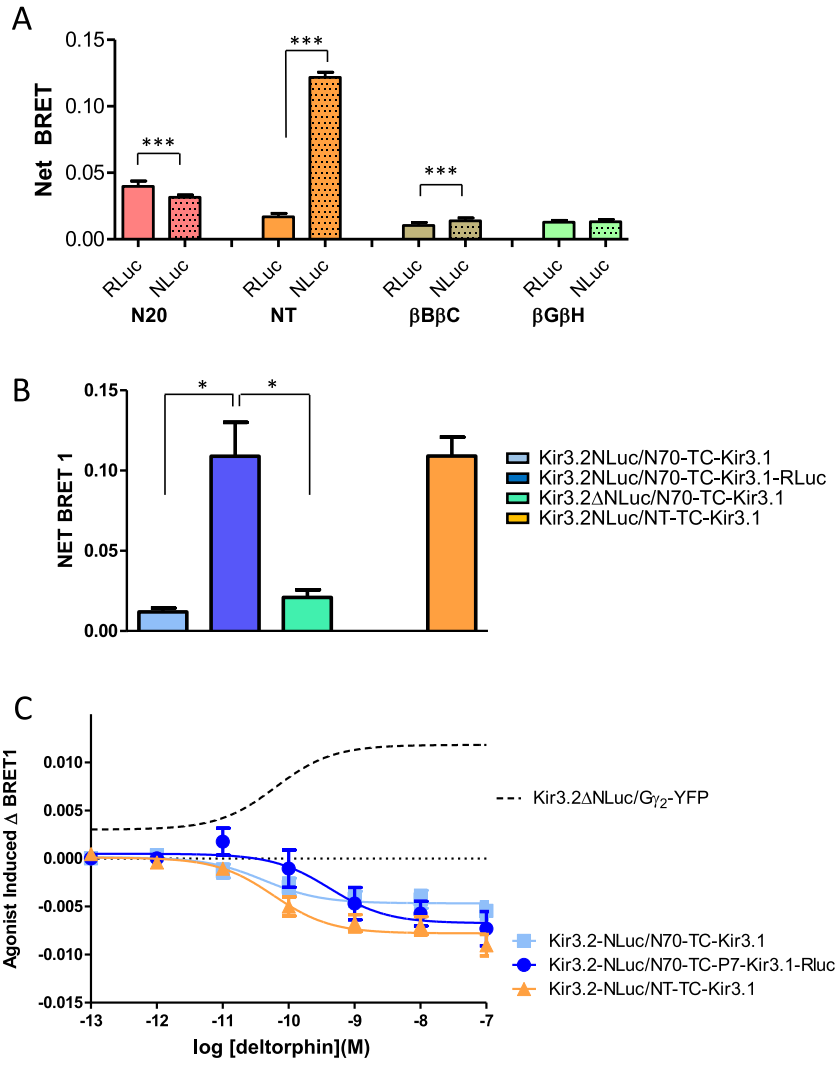

Fig. 6. Characterization of BRET signals generated by intermolecular Kir3.2-NLuc/Kir3.1-TC pairs. (A) Basal net BRET was monitored in HEK 293 cells expressing δORs, either Kir3.2-RLuc or Kir3.2-NLuc, together with indicated Kir3.1-TC constructs and complementary signaling partners ($G\alpha_o\beta_1\gamma_2$ + untagged Kir3.1/Kir3.2). Data represent mean net BRET ± SEM and correspond to 11–15 independent experiments. They were analyzed by two way ANOVA which showed an effect of RLuc vs NLuc ($p < 0.001$), of acceptor location ($p < 0.001$) and an interaction ($p < 0.001$). Post hoc analyses revealed significant increases in net BRET for pairs containing Kir3.2-RLuc, as shown in the figure. (B) Cells were transfected with the indicated N70-TC-Kir3.1 donor constructs, either Kir3.2-NLuc or Kir3.2-ΔNLuc together with signaling partners as in (A). *Note:* Kir3.2-NLuc/NT-TC-Kir3.1 was monitored in parallel for comparison. Data represent mean net BRET ± SEM and correspond to 3–10 independent experiments. They were analyzed by one way ANOVA ($p < 0.01$) and post hoc analysis indicated differences in biosensors as indicated in the figure. (C) HEK 293 cells transfected as above were exposed to increasing concentrations of deltorphin B as indicated, and BRET measures taken 2 min after drug exposure. Data represent mean ΔBRET ± SEM of 5–13 independent experiments. FlAsH-TC BRET data were analyzed by two way ANOVA which showed an effect of concentration ($p < 0.001$), an effect of biosensor ($p < 0.01$) and no interaction. Post-hoc comparisons indicated significant effects at the three highest concentrations for all three biosensors ($^{*}p < 0.001$).

Please cite this article in press as: D.N. Robertson et al., Methods (2015), http://dx.doi.org/10.1016/j.ymeth.2015.07.011

(not shown), and was therefore not further pursued. N70-TC-Kir3.1-RLuc was then co-expressed with Kir3.2-NLuc and quite to our surprise the biosensor resulting from this combination displayed a basal net BRET signal similar to that of Kir3.2-NLuc/NT-TC-Kir3 (Fig. 6B), the best pair we had tested thus far. This rather peculiar biosensor was also sensitive to deltorphin B which caused basal net BRET to fall by 0.007 ± 0.001 arbitrary units ($n = 5$; $p < 0.001$; Fig. 6C). Importantly, despite its improved dynamic window, Kir3.2-NLuc/N70-TC-Kir3.1-RLuc cannot be considered a good biosensor to locate conformational changes imposed by different channel activators. On the other hand, it proved most useful in the characterization of BRET kinetics (Section 3.9).

3.8.2. Pharmacological profile of FlAsH-TC-Kir3.1/Kir3.2-NLuc biosensors

The Kir3.2-NLuc/NT-TC-Kir3.1 pair was chosen to determine if ligand-induced changes in BRET faithfully reproduced known Kir3 channel pharmacology. However, before comparisons among different channel activators were carried out, it was necessary to assess whether biosensors that captured channel activation from different vantage points consistently reported pharmacological parameters for a specific ligand. As shown in Fig. 6C, deltorphin B induced concentration-dependent changes in BRET in three different Kir3.2-NLuc/FlasH-TC-Kir3.1 biosensors which monitored conformational changes within the N-terminal portion of the channel. Comparison of EC_{50} values obtained with traditional pairs such as Kir3.2-NLuc/NT-TC-Kir3.1 and Kir3.2-NLuc/N70-TC-Kir3.1, confirmed reasonable agreement among the two parameters (Table 3), which were also consistent with responses previously reported for deltorphin B [33]. Moreover, deltorphin's potency on these channel pairs was not different from that observed with another biosensor reporting channel activation by GPCR ligands [8], which monitors conformational changes at the interface of the Gβγ dimer and channel subunits (Kir3.2-ΔNLuc/YFP-Gγ2; Figs. 5A and 6C). Deltorphin's EC_{50} on the pair containing the FlAsH-TC acceptor together with RLuc and NLuc donors (Kir3.2-NLuc/N70-TC-Kir3.1-RLuc) was shifted to the right by one order of magnitude (Table 3), which is not unexpected given multiple modifications of channel proteins. Finally, differences in maximal BRET changes induced by deltorphin B in the different pairs (Table 3) was consistent with the biosensors having different dynamic windows. Taken together, these results indicate that different biosensors were similarly able to monitor concentration-dependent effects of a δOR ligand on the Kir3 channel.

We then addressed whether the biosensors could discriminate between δOR agonists that are expected to display different potencies. Thus, cells expressing Kir3.2-NLuc/NT-TC-Kir3.1 together with complementary signaling partners were exposed to AR-M 390 and morphine, δOR agonists with distinct affinities for δORs [34,35] (Fig. 7A). The dose–response curves were compared to those obtained with a validated, classical, $G\alpha_o$-Luc/GFP-$G\gamma_2$ biosensor that allows monitoring of G protein activation in live cells [33,36,37] (Fig. 7A, *inset*). $G\alpha_{oA}$ was chosen for comparison as it was the subtype co-expressed with the channel biosensor. The

Table 3
Characterization of deltorphin B responses in different Kir3.1-NLuc/Kir3.1-TC pairings.

Construct	EC_{50} (pM)	*E*max
Kir3.2-NLuc/NT-TC-Kir3.1 ($n = 19$)	63.1 ± 1.23	−0.009 ± 0.001
Kir3.2-NLuc/N70-TC-Kir3.1 ($n = 13$)	39.8 ± 1.52	−0.005 ± 0.001
Kir3.2-NLuc/N70-TC-Kir3.1-RLuc ($n = 5$)	3.98 ± 0.169	−0.007 ± 0.001
Kir3.2-ΔNluc/YFP-Gγ2 ($n = 6$)	63.1 ± 3.09	+0.009 ± 0.002

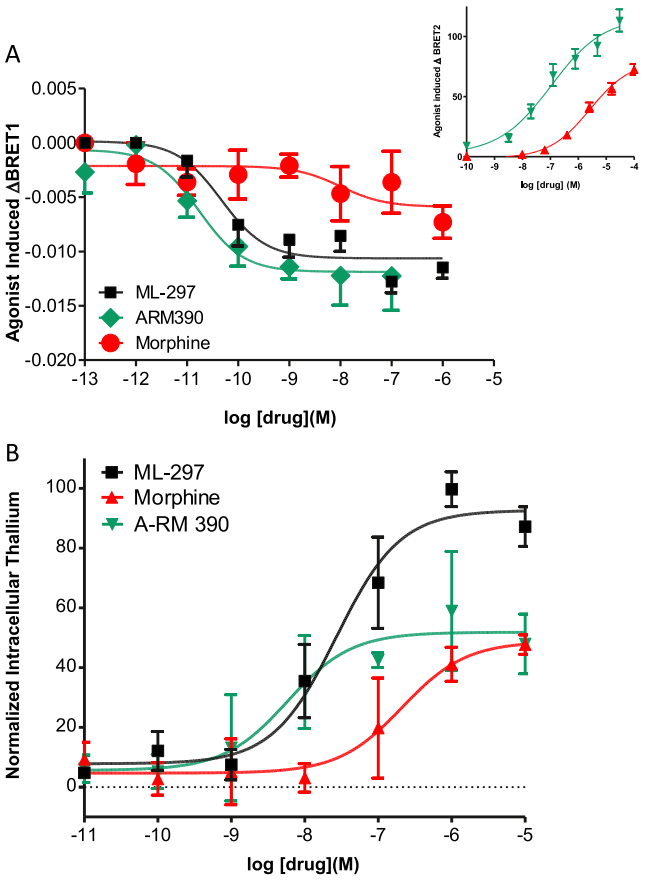

Fig. 7. Characterization of pharmacological responses produced by Kir3.2-NLuc/NT-TC-Kir3.1 biosensors. (A) Basal net BRET was monitored in HEK 293 cells expressing δORs, Kir3.2-NLuc/NT-TC-Kir3.1 pair together with complementary signaling partners ($G\alpha_o\beta_1\gamma_2$ + untagged Kir3.1/Kir3.2) and were exposed to increasing concentrations of the indicated ligands. Data represent mean ΔBRET ± SEM of 5–8 independent experiments. Curves were analyzed by two-way ANOVA which revealed an effect of drug ($p < 0.001$), an effect of concentration ($p < 0.01$) and no interaction. Post-hoc comparisons indicated that morphine was significantly different from ML-297 and AR-M 390 at the three highest concentrations ($^*p < 0.05$). *Inset:* HEK 293 cells transfected with δORs, the $G\alpha_o$-Luc/GFP-$G\gamma_2$ BRET pair and complementary $G\beta_1\gamma_2$ subunits were exposed to morphine or AR-M 390. Curves were compared by two-way ANOVA showing an effect of drug ($p < 0.001$), an effect of concentration ($p < 0.01$) and no interaction. (B) HEK 293 cells stably expressing δORs and Kir3.1/Kir3.2 subunits were labeled with thallium, and exposed to increasing concentrations of indicated ligands before fluorescence measures were taken. Results correspond to mean ± SEM of 3–7 experiments carried out in duplicate. And represent changes in fluorescence normalized to ML-297. Curves were compared by two-way ANOVA, revealing an effect of drug ($p < 0.001$), an effect of concentration ($p < 0.01$) and no interaction. Post hoc comparisons indicated that ML-297 was significantly different from morphine and AR-M 390 at the three and two highest concentrations, respectively ($p < 0.05$).

rank order of EC_{50} values was conserved at the two stages of signal transduction, morphine being less potent than AR-M 390 (Table 4), an observation consistent with the rank order of affinities for the receptor [33–35,38].

In addition to being physiologically activated via GPCRs, Kir3 channels are stimulated by ligands that bind directly to the channel [29,30]. ML-297, a member of a new family of small molecules which specifically recognizes residues F137 and D173 present only in Kir3.1 subunits [13], was chosen as a direct channel activator. BRET effects produced by ML-297 were not different from those observed with AR-M 390, its potency similarly falling within the pM range (Table 4). Such high potency was quite surprising since the reported EC_{50} for ML-297 in modulating Kir3.1/Kir3.2 channel activity was three orders of magnitude lower [13,30]. This difference between BRET and functional studies cannot be attributed

Table 4
Characterization of the pharmacological profile of the Kir3.2-NLuc/NT-TC-Kir3.1 pairing in different assays.

Assay Ligand	G protein activation α_0A-Luc/GFPγ2 EC_{50}	Channel biosensor Kir3.2-NLuc/NT-TC-Kir3.1 EC_{50}	Voltage-sensitive dye: Fluxor EC_{50}
Morphine	2 ± 0.1 μM (n = 3)	10 nM ± 1 nM (n = 7)	199 ± 2 nM (n = 3)
AR-M 390	63 ± 0.9 nM (n = 3)	15.8 pM ± 0.58 (n = 8)	10 ± 1 nM (n = 6)
ML-297	N/A	46.77 pM ± 1.36 (n = 5)	32 ± 1 nM (n = 7)

to an effect of the solvent DMSO on the signal since its concentration was kept constant across all points of the ML-297 dose response curve (see Supplementary Fig. 4 for solvent effects on NLuc/FlAsH-TC signals). Thus, in order to better understand the differences between BRET readouts and reported functional studies, we compared BRET responses of all three ligands to those obtained using the Fluxor® system (Fig. 7B). This fluorometric assay of channel activity was where ML-297 activity was initially tested [30]. Interestingly, the rank order of ligand potency to reduce BRET and to increase thallium fluorescence were maintained, but all EC_{50} values were right-shifted by 2–3 orders of magnitude (Table 4). This shift clearly points to overall differences in assay sensitivity to drug actions. These differences may stem from the fact that BRET biosensors provide a direct readout of the channel while voltage-sensitive dyes report activity several steps downstream of the channel. It is also worth noting that while the conformational response to ML-297 was of similar magnitude as AR-M 390, its functional Fluxor® response was ~45% greater. One possible explanation for this observation is simply the distinct nature of both assays. While BRET offers a direct readout of conformational changes associated with K^+ ion flux Fluxor® is a thallium based assay. ML-297 binds to residues on the channel pore, so the way both assays capture its effects may not necessarily be the same.

3.9. Time course of BRET responses vs channel currents

BRET-based tools to monitor conformational rearrangements of ion channels provide a direct estimation of channel activity that is closer to electrophysiological recordings than indirect cell-based methods which rely on voltage-dependent dyes. Because conformational reorganization supports changes in ion permeability, the expectation was to find correspondence in the kinetics of responses captured by BRET biosensors and channel current. Thus, to verify whether this was the case two sets of cells were transfected with the (Kir3.2-NLuc/N70-TC-Kir3.1-RLuc) biosensor and corresponding signaling partners, where one was used for BRET and the other in whole cell patch clamp assays. In both cases, cells were exposed to 10 μM Met-Enkephalin which was left in the incubation medium until the end of the assay. Fig. 8A and B shows immediate changes in BRET and channel currents upon introduction of the δOR agonist. The time course of these changes followed first order kinetics with a $t_{1/2}$ of 2.8 s (tau 4.1 ± 0.5). Note that while single channel bursts occur on a millisecond time scale, BRET monitors the kinetics of all channels present in a population of cells. Nonetheless, the time course of BRET changes was in reasonable agreement with whole-cell current kinetics ($t_{1/2}$ = 2.1 s, tau 3.1 ± 0.3).

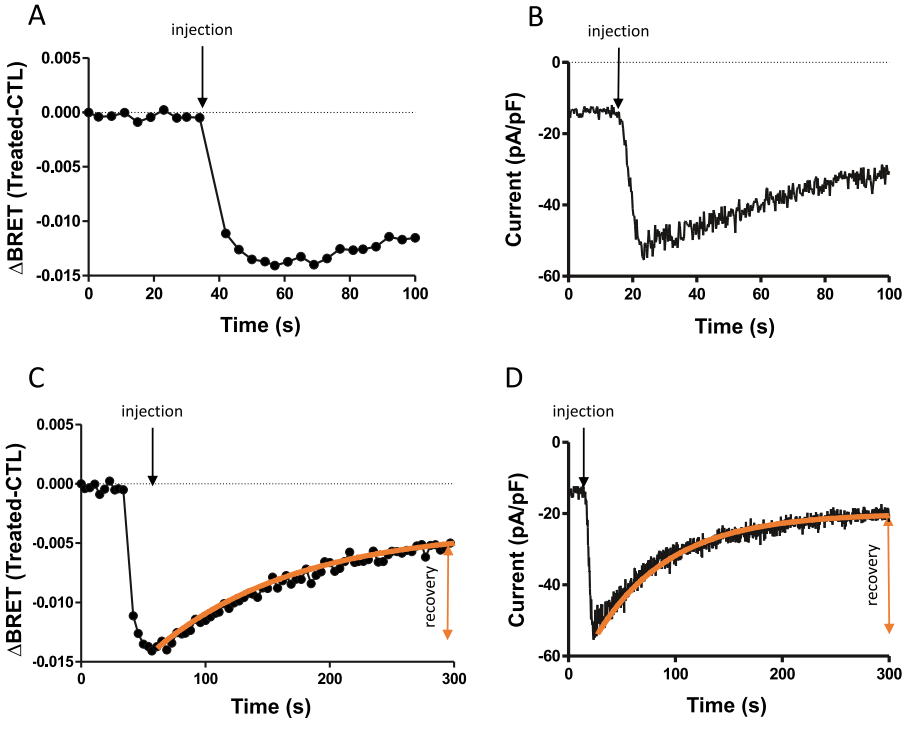

Fig. 8. The time course of conformational changes monitored by BRET biosensors parallels that of channel currents. HEK 293 cells were transfected with δORs, Kir3.2-Luc/N70-TC-Kir3.1-RLuc and complementary signaling partners as above, and used to assess activation-induced BRET changes (A and C) or channel currents (B and D). Arrow represents injection of δOR agonist Met-Enkephalin (10 μM), which was left in the incubation medium throughout the recordings. (A) Time course of BRET for the initial 100 s after injection with agonist: $t_{1/2}$ 2.8 s; tau = 4.1 ± 0.5 s. (B) Time course of channel currents for the initial 100 s after injection with agonist: $t_{1/2}$ = 2.1 s, tau = 3.1 ± 0.3 s. (C) Time course of BRET response for the initial 300 s after injection with agonist, shows 77% recovery of basal signal: $t_{1/2}$ = 93 s; tau = 134 ± 8 s. (D) Time course of channel currents for the initial 300 s after injection with agonist, shows 82% recovery of basal signal: $t_{1/2}$ = 60 s; tau = 134 ± 8 s.

Once BRET changes had attained their maximum decrease, the signal recovered, though not completely (Fig. 8C and D). The kinetics of recovery were much slower ($t_{1/2}$ = 93 s; Tau 134 ± 8) than those observed upon activation, and recovery after 5 min recording was incomplete (~77% of basal energy transfer). The generated current decayed in a similar time frame as the BRET signal, reaching 28% of its initial value with $t_{1/2}$ = 60 s (tau 134 ± 8). Thus, the close correspondence in BRET and current kinetics supports our claim that this conformational tool captures channel rearrangements underlying current flow.

4. Discussion

Here, we used Kir3 family channels as prototypes to design and develop FlAsH/BRET-based conformational biosensors to monitor real-time rearrangements among channel subunits as they become activated. The approach taken involved a systematic series of protein engineering and validation steps including verification of membrane expression and current conductance to produce functionally-competent biosensors that captured conformational changes associated with channel activation. Biosensor positioning was guided by recent structural studies of Kir3 channels [19,39,40] so as to introduce donor–acceptor pairs into positions that undergo conformational changes during channel opening while avoiding regions associated with the activation mechanism *per se*. The larger donor moiety was always located at the C-terminal end of either Kir3.1 (intramolecular biosensors) or Kir3.2 (intermolecular biosensors) subunits while the smaller FlAsH-binding TC domain was introduced at alternative positions within the NTD (NT, N20 and N70), or within cytosolic loops of the Kir3.1 channel subunits (βBβC and βGβH). RLuc and NLuc were both explored as possible donors, always using h coelenterazine as a substrate to generate luminescence within the excitation wavelength of the TC-FlAsH fluorophore (max = 508 nm).

The RLuc system proved useful in demonstrating that the FlAsH–BRET approach could discriminate donor positions 20 residues apart, as evidenced by differences in basal energy transfer recorded between NT-Kir3.1 and N20-Kir3.1 TC-domain constructs. This type of approach has also been used to "walk" TC tags through the intracellular loops of a GPCR [28] (this issue). The RLuc donor system also allowed us to corroborate that changes in BRET could be a good surrogate of channel activity. Indeed, channel activation is accompanied by a clockwise rotational movement of the CTD with respect to the plane of the membrane, where N and C-terminal ends of the same subunit approach one another while those on neighboring subunits separate [19,20,41]. BRET increases observed after activation of NT or N20-tagged intramolecular biosensors and decreases at corresponding intermolecular ones, were consistent with this rotation taking place, and with previous spectroscopic reports of the same rearrangement using canonical FRET pairs [42].

Despite the ability to capture conformational changes that take place during channel activation, the RLuc system displayed low basal BRET signals and considerable variability in ligand-induced changes prompting us to the optimize an alternative donor system. NLuc [17] proved beneficial in increasing basal BRET and improving the dynamic window of the intermolecular biosensors previously tested with RLuc. Thus, the activation of the biosensor containing the NT-Kir3.1 acceptor moiety in combination with the Kir3.2-NLuc donor also resulted in BRET reduction, as did the activation of a novel pair constituted by N70-Kir3.1/Kir3.2-NLuc. Introduction of the TC-tag at this location was intended to capture the movement that takes place at the interfacial helix near the helix bundle crossing, a displacement associated with changes in the conducting state of the KirBac channel [20]. Thus, although of smaller magnitude than the one observed at NT-Kir3.1/Kir3.2-NLuc, the activation-driven BRET change at this new position was also consistent with a crystal-based model of Kir channel activation [20].

By capturing conformational changes associated with channel activation these biosensors provide a direct, non-electrophysiological readout of channel function that could eventually be adapted in a cell-based assay to screen for channel modulators and/or characterize ligands in terms of distinct conformational changes they might evoke. For either of these applications it was important to determine whether the biosensor readout mimicked validated pharmacological responses. In this sense we were able to show that the potency of deltorphin B to affect BRET between the Gβγ dimer and Kir3 subunits, a previously validated conformational read-out of channel activation by GPCR ligands [8], was similar to the potency displayed to alter BRET in Kir3.2-Luc/NT-TC-Kir3.1 and Kir3.2-Luc/N70-TC-Kir3.1 pairs. The concordance of the validated Gβγ/Kir3 readout with the potency obtained in a pair of constructs bearing more important modifications to their structure (N70-Kir3.1-RLuc/Kir3.2-Luc) was not exact, but was within the range of variation of EC_{50} estimates (whose SEM corresponded to ~15% the value of these parameters). The Kir3.2-Luc/NT-TC-Kir3.1 biosensor was further tested for its ability to discriminate between AR-M 390 and morphine, which are respectively known to evoke high (nM range) [34,35] and low (μM range) [33,38] potency responses at δORs. Consistent with this, AR-M 390 was ~100 fold more potent than morphine in modifying basal net BRET in Kir3.2-Luc/NT-TC-Kir3.1, a rank order maintained in both upstream ($G\alpha_{oA}$ activation) and downstream (Fluxor®) functional assays. Similar to AR-M 390, ML-297 potency at the NT-TC-Kir3.1/Kir3.2-Luc biosensor was within the pM range but EC_{50} values for both ligands were right-shifted by three orders of magnitude in the Fluxor® assay, falling within the same nM range of other functional responses reported for both ligands [30,43]. The reason for this system-related difference in sensitivity is not yet clear, but it was also observed, though to a lesser extent, for morphine.

Mechanistically, how ML-297 and GPCR ligands activate Kir3 family channels is quite distinct. GPCR-mediated activation of the G protein prompts the interaction between the "hot spot" on Gβ [44] and residues in the βL-βM sheet of one Kir3 subunit and the N-terminus and βD-βE sheet of the neighboring one. This rearrangement causes a partial opening of the channel at the "G loop" girdle and enhances the channel's affinity for PIP_2 which, upon binding, triggers additional opening of the inner helical crossing [19]. By binding to residues in the pore and M2 inner helices, ML-297 produces the opening of both gates [13]. We observed that ML-297 modified energy transfer at a cytosolic biosensor, implying that conformational information is transmitted from the transmembrane path to CTDs. In support of this interpretation is crystallographic data showing concordant movements at the selectivity filter and cytosolic domains [20]. Independent of the mechanism involved, the practical consequence of this observation is that a biosensor which, like Kir3.2-NLuc/NT-TC-Kir3.1, monitors rotational movement of transmembrane domains does not discriminate among ligands with distinct activation mechanisms. The notion that Kir3.2-Luc/NT-TC-Kir3.1 is a universal biosensor of channel activation is further supported by the fact that propanol also reduced RET at this interface (Supplementary Fig. 5). Similar to other a short chain alcohols, propanol activates the channel in a G protein-independent manner by binding to a pocket delimited by N-terminus, βD-βE and βL-βM sheets [29,45]. Thus, if we are to discriminate among activation mechanisms of different ligands, additional conformational vantage points are needed. For example, we could speculate that BRET pairs which capture movements of βL-βM or βD-βE sheets, would be sensitive to conformational

rearrangements caused by short-chain alcohols and Gβγ but not ML-297. Moreover, one would predict that a pair which monitors the Gβγ/Kir3 would discriminate among alcohol and GPCR-mediated activation. In this scenario, a channel-activating drug can be described by a conformational footprint generated from multiple complementary biosensors.

Finally, the observation that BRET readings and channel currents showed similar kinetics indicates that using conformational channel biosensors offers adequate temporal resolution to monitor channel activity. Indeed, changes in BRET provided insight into both the rapid activation and the slower phase of signal decay. In relation to the latter it is interesting to note that β-arrestin$_2$ (βarr$_2$) recruitment to δORs occurs with $t_{1/2}$ = 50–80 s [46], so it is tempting to speculate that the BRET recovery phase may correspond to conformational changes undergone by channel subunits as δOR interactions with βarr interfere with channel activation. Furthermore, since recent data indicate that δORs and Kir3 channels may remain associated during βarr$_2$ recruitment and subsequent internalization [47], it is also possible that BRET measured during the recovery phase may result from direct interaction of βarr with complex components.

In summary, we have outlined the different steps involved in design, construction and validation of Kir3 conformational biosensors which directly track structural rearrangements undergone by channel proteins via changes in RET. The responses observed displayed temporal resolution and a pharmacological profile that are compatible with those obtained by other methods for the same channels. The possibility of adapting this approach to other channels and the potential for developing simple cell-based assays that provide direct conformational information of channel activity is promising, and should also provide new insight not only on the pharmacology but on how these signaling proteins function and are regulated.

Acknowledgments

This research was supported by grants from the Natural Sciences and Engineering Research Council of Canada NSERC (311997) (G.P.) and the Consortium Québécois pour le Développement de médicaments (CQDM) through their EXPLORE program (G.P.).

Appendix A. Primers for constructs containing RLuc and TC-domain tags for performing intra-molecular BRET

NT: Acc65I Kozak ATG FlAsH Kir3.1 FWD: 5′-tatggtaccgccaccatgtgctgccccggctgctgcatgtctgcactccgaagg-3′; Kir3.1 BamHI RVS: 5′-gccggatcctgtgaagcgatcagagttc-3′.

N20: Fragment 1, ACC65I Kozak Kir3.1 FWD: 5′-tatggtaccgccaccatgtctgcactcc-3′; FlAsH Kir3.1N-terminus (20) RVS: 5′-gcagcagccggggcagcagctggacgatgtggtcac-3′. Fragment 2, FlAsH Kir3.1N-terminus (20) FWD: 5′-tgctgccccggctgctgcggctcgggcttgcagccc-3′; Kir3.1 BamHI RVS: 5′-gccggatcctgtgaagcgatcagagttc-3′.

N70: Fragment 1, ACC65I Kozak Kir3.1 FWD: 5′-tatggtaccgccaccatgtctgcactcc-3′; N-term N70 RVS: 5′-gcagcagccggggcagcacaggttgccgtgctgtac-3′. Fragment 2, N-term N70 FWD: 5′-tgctgccccggctgctgcggcagcgagacaagccgc-3′; Kir3.1 STOP BamHI RVS: 5′-gccggatccttatgtgaagcgatcagagttc-3′.

βB-βC: Fragment 1, ACC65I Kozak Kir3.1 FWD: 5′-tatggtaccgccaccatgtctgcactcc-3′; FlAsH Kir3.1 betaB-betaC RVS: 5′-gcagcagccgggcagcacatggagatcaccgcgtg-3′. Fragment 2, FlAsH Kir3.2 betaB-betaC FWD: 5′-tgctgccccggctgctgcagggacgaaaactcacg-3′; Kir3.1 BamHI RVS: 5′-gccggatcctgtgaagcgatcagagttc-3′.

βG-βH: Fragment 1, ACC65I Kozak Kir3.1 FWD: 5′-tatggtaccgccaccatgtctgcactcc-3′; FlAsH Kir3.1 betaG-betaH RVS: 5′-gcagcagccgggcagcaataaaaggggcttttggc-3′. Fragment 2, FlAsH Kir3.1 betaG-betaH FWD: 5′-tgctgccccggctgctgcgacctatcccagcgaagc-3′; Kir3.1 *BamHI RVS:* 5′-gccggatcctgtgaagcgatcagagttc-3′.

Appendix B. Primers for acceptor constructs containing TC-domain tags for performing inter-molecular BRET

NT: Acc65I Kozak ATG FlAsH Kir3.1 FWD: 5′tatggtaccgccaccatgtgctgccccggctgctgcatgtctgcactccgaagg-3′; Kir3.1 STOP BamHI RVS: 5′-gccggatccttatgtgaagcgatcagagttc-3′.

N20: Fragment 1, ACC65I Kozak Kir3.1 FWD: 5′-tatggtaccgccaccatgtctgcactcc-3′; FlAsH Kir3.1N-terminus (20) RVS: 5′-gcagcagccggggcagcagctggacgatgtggtcac-3′. Fragment 2, FlAsH Kir3.1N-terminus (20) FWD: 5′-tgctgccccggctgctgcggctcgggcttgcagccc-3′; Kir3.1 STOP BamHI RVS: 5′-gccggatccttatgtgaagcgatcagagttc-3′.

N70: Fragment 1, ACC65I Kozak Kir3.1 FWD: 5′-tatggtaccgccaccatgtctgcactcc-3′; N-term N70 RVS: 5′-gcagcagccggggcagcacaggttgccgtgctgtac-3′. Fragment 2, N-term N70 FWD: 5′-tgctgccccggctgctgcggcagcgagacaagccgc-3′; Kir3.1 STOP BamHI RVS: 5′-gccggatccttatgtgaagcgatcagagttc-3′.

βB-βC: Fragment 1, ACC65I Kozak Kir3.1 FWD: 5′-tatggtaccgccaccatgtctgcactcc-3′; FlAsH Kir3.1 betaB-betaC RVS: 5′-gcagcagccgggcagcacatggagatcaccgcgtg-3′. Fragment 2; FlAsH Kir3.2 betaB-betaC FWD: 5′-tgctgccccggctgctgcagggacgaaaactcacg-3′; Kir3.1 STOP BamHI RVS: 5′-gccggatccttatgtgaagcgatcagagttc-3′.

βG-βH: Fragment 1, ACC65I Kozak Kir3.1 FWD: 5′-tatggtaccgccaccatgtctgcactcc-3′; FlAsH Kir3.1 betaG-betaH RVS: 5′-gcagcagccgggcagcaataaaaggggcttttggc-3′. Fragment 2, FlAsH Kir3.1 betaG-betaH FWD: 5′-tgctgccccggctgctgcgacctatcccagcgaagc-3′; Kir3.1 STOP BamHI RVS: 5′-gccggatccttatgtgaagcgatcagagttc-3′.

Appendix C. Supplementary data

Supplementary data associated with this article can be found, in the online version, at http://dx.doi.org/10.1016/j.ymeth.2015.07.011.

References

[1] A. Wickenden, B. Priest, G. Erdemli, Future Med. Chem. 4 (5) (2012) 661–679.
[2] A. Picones, Curr. Top. Med. Chem. 15 (7) (2015) 631–637.
[3] Y. Du et al., ACS Chem. Neurosci. (2015).
[4] P. Kofuji, N. Davidson, H.A. Lester, Proc. Natl. Acad. Sci. U.S.A. 92 (14) (1995) 6542–6546.
[5] D.E. Keith et al., J. Biol. Chem. 271 (32) (1996) 19021–19024.
[6] R.V. Rebois et al., Cell. Signal. 24 (11) (2012) 2051–2060.
[7] N. Lavine et al., J. Biol. Chem. 277 (48) (2002) 46010–46019.
[8] M. Richard-Lalonde et al., Mol. Pharmacol. 83 (2) (2013) 416–428.
[9] E. Goupil et al., J. Biol. Chem. 285 (33) (2010) 25624–25636.
[10] C. Hoffmann et al., Nat. Protoc. 5 (10) (2010) 1666–1677.
[11] H. Hibino et al., Physiol. Rev. 90 (1) (2010) 291–366.
[12] C. Luscher, P.A. Slesinger, Nat. Rev. Neurosci. 11 (5) (2010) 301–315.
[13] N. Wydeven et al., Proc. Natl. Acad. Sci. U.S.A. 111 (29) (2014) 10755–10760.
[14] K. Nagi, G. Pineyro, Front. Cell. Neurosci. 8 (2014) 186.
[15] J.G. McCoy, C.M. Nimigean, Biochim. Biophys. Acta 1818 (2) (2012) 272–285.
[16] A.M. Loening, T.D. Fenn, S.S. Gambhir, J. Mol. Biol. 374 (4) (2007) 1017–1028.
[17] M.P. Hall et al., ACS Chem. Biol. 7 (11) (2012) 1848–1857.
[18] C. Hoffmann et al., Nat. Methods 2 (3) (2005) 171–176.
[19] M.R. Whorton, R. MacKinnon, Nature 498 (7453) (2013) 190–197.
[20] O.B. Clarke et al., Cell 141 (6) (2010) 1018–1029.
[21] O. Schoots et al., Cell. Signal. 11 (12) (1999) 871–883.
[22] Y. Shi et al., Neurosci. Res. 36 (3) (2000) 209–214.
[23] G. Krapivinsky et al., Nature 374 (6518) (1995) 135–141.
[24] Y.J. Liao, Y.N. Jan, L.Y. Jan, J. Neurosci. 16 (22) (1996) 7137–7150.
[25] D. Ma et al., Neuron 33 (5) (2002) 715–729.
[26] K.D. Pfleger, K.A. Eidne, Nat. Methods 3 (3) (2006) 165–174.
[27] P. Zylbergold et al., Front. Cell. Neurosci. 8 (2014) 108.
[28] R. Sleno et al., Methods (2015) (current issue).
[29] P. Aryal et al., Nat. Neurosci. 12 (8) (2009) 988–995.
[30] K. Kaufmann et al., ACS Chem. Neurosci. 4 (9) (2013) 1278–1286.
[31] H. Dacres et al., Biochem. Biophys. Res. Commun. 425 (3) (2012) 625–629.
[32] F.F. Hamdan et al., J. Biomol. Screen. 10 (5) (2005) 463–475.
[33] H.B. Tudashki et al., Mol. Pharmacol. 85 (1) (2014) 148–161.
[34] N. Plobeck et al., J. Med. Chem. 43 (21) (2000) 3878–3894.

[35] Z.Y. Wei et al., J. Med. Chem. 43 (21) (2000) 3895–3905.
[36] N. Audet et al., J. Biol. Chem. 283 (22) (2008) 15078–15088.
[37] C. Gales et al., Nat. Struct. Mol. Biol. 13 (9) (2006) 778–786.
[38] I. Charfi et al., Cell. Mol. Life Sci. 71 (8) (2014) 1529–1546.
[39] M. Nishida et al., EMBO J. 26 (17) (2007) 4005–4015.
[40] M.R. Whorton, R. MacKinnon, Cell 147 (1) (2011) 199–208.
[41] R. Sadja et al., Neuron 29 (3) (2001) 669–680.
[42] I. Riven et al., Neuron 38 (2) (2003) 225–235.
[43] A.A. Pradhan et al., PLoS One 4 (5) (2009) e5425.
[44] J.K. Scott et al., EMBO J. 20 (4) (2001) 767–776.
[45] T. Kobayashi et al., Nat. Neurosci. 2 (12) (1999) 1091–1097.
[46] N. Audet et al., J. Neurosci. 32 (14) (2012) 4827–4840.
[47] K. Nagi, I. Charfi, G. Pineyro, Cell. Mol. Life Sci. (2015).

Please cite this article in press as: D.N. Robertson et al., Methods (2015), http://dx.doi.org/10.1016/j.ymeth.2015.07.011